Cy 2

EVALUATION OF A MASS SPECTROMETER PROBE FOR DENSITY AND VELOCITY DISTRIBUTION MEASUREMENTS IN A ROCKET EXHAUST PLUME

H. M. Powell, D. W. Hill, and D. L. Whitfield

ARO, Inc.

September 1971

Approved for public release; distribution unlimited.

VON KÁRMÁN GAS DYNAMICS FACILITY
ARNOLD ENGINEERING DEVELOPMENT CENTER
AIR FORCE SYSTEMS COMMAND
ARNOLD AIR FORCE STATION, TENNESSEE

NOTICES

When U. S. Government drawings specifications, or other data are used for any purpose other than a definitely related Government procurement operation, the Government thereby incurs no responsibility nor any obligation whatsoever, and the fact that the Government may have formulated, furnished, or in any way supplied the said drawings, specifications, or other data, is not to be regarded by implication or otherwise, or in any manner licensing the holder or any other person or corporation, or conveying any rights or permission to manufacture, use, or sell any patented invention that may in any way be related thereto.

Qualified users may obtain copies of this report from the Defense Documentation Center.

References to named commercial products in this report are not to be considered in any sense as an endorsement of the product by the United States Air Force or the Government.

EVALUATION OF A MASS SPECTROMETER PROBE FOR DENSITY AND VELOCITY DISTRIBUTION MEASUREMENTS IN A ROCKET EXHAUST PLUME

H. M. Powell, D. W. Hill, and D. L. Whitfield
ARO, Inc.

FOREWORD

The work reported herein was sponsored by Arnold Engineering Development Center (AEDC), Air Force Systems Command (AFSC), under Program Element 64719F.

The results presented were obtained by ARO, Inc. (a subsidiary of Sverdrup & Parcel and Associates, Inc.), contract operator of AEDC, AFSC, Arnold Air Force Station, Tennessee, under Contract F40600-72-C-0003. The work was conducted from October 17, 1969, to June 1970 under ARO Projects VW3008 and ST1027. The manuscript was submitted for publication on March 15, 1971.

This technical report has been reviewed and is approved.

B. B. Algee
Major, CF
Research and Development Division
Directorate of Technology

Harry L. Maynard
Colonel, USAF
Director of Technology

ABSTRACT

The evaluation of a mass spectrometer probe in a highly expanded exhaust plume of a small rocket is described in this report. This probe, which utilizes a quadrupole mass spectrometer, is used for species identification and concentration measurements and for velocity distribution measurements. The probe maintains a compatible pressure environment for the spectrometer during rocket firings and generates a molecular beam which is representative of the plume gas dynamic state at a given sampling point. The modulated beam technique for both density and velocity distribution measurements is described. The important criteria for the design of the more important features are discussed. Sample data from calibration sources and the thruster are presented along with analysis of the data as it relates to parameter spatial dependence and kinetic temperatures calculated from the velocity distributions. Some observations concerning the thruster chemical and gas dynamic properties are presented and compared with certain theoretical properties. This comparison is useful in evaluating the performance of the probe. The problem areas in both the probe and instrumentation performance are discussed with suggestions for improvements in the system.

CONTENTS

APPENDIXES

I. ILLUSTRATIONS

Figure

SECTION I
INTRODUCTION

There is a current need for certain gas dynamic measurements in highly expanded rocket exhausts. These measurements relate to such studies as plume chemical and gas dynamic characteristics, plume effects on surfaces and bodies, plume-to-plume and plume-to-free-stream interactions, plume radiation effects, and others. The identification of molecular species in the exhaust plume, concentrations and/or relative densities, velocity distribution functions, and gas properties derived from the various moments of the distribution function are useful for evaluating these plume effects. The spatial dependence of these parameters is also of particular interest. A mass spectrometer probe that provides a means of determining the chemical and gas dynamic state of a rocket exhaust has been the object of considerable developmental effort. This report is intended to describe the technique and the evaluation of the probe performance.

The probe evaluation was conducted in the Aerospace Research Chamber (10V) of the Aerospace Division of the von Kármán Gas Dynamics Facility (VKF). The test simulated orbital or near-orbital conditions and was conducted with a small, scaled thruster. In addition to the probe evaluation, some rather significant results were obtained for the rocket performance. The rocket combustion characteristics as determined by the mass spectrum and as a function of oxidizer/fuel (O/F) ratios, as well as the translational kinetic temperatures and speed ratios obtained from appropriate moments of the measured velocity distribution functions, are of particular interest.

SECTION II
DESCRIPTION OF THE TECHNIQUE

2.1 BASIC PROBE CONFIGURATION

Because of the many species involved, a mass spectrometer is the heart of the system to be described. Conventional mass discrimination is used in measurements of gas species concentrations and velocity distributions. Quadrupole mass spectrometers, because of their size, shape, and weight are well suited to these applications. The mass range of interest is from 1 to 47 atomic mass units (amu). This mass range accounts for 99 percent of all gas species studied in this evaluation.

Because of the relatively high gas densities in the plume, a sampling orifice probe is required for the mass spectrometer. The principal requirement is that a low gas pressure ($< 10^{-5}$ torr) be assured that is compatible with linear operation of the quadrupole. This was done by pumping on the probe directly with sufficient speed to handle the gas load from the plume and the chamber background. One such design is shown in Fig. 1, Appendix I. This design has been guided by the need to keep the pressure as low as possible inside the probe and minimize molecular scattering effects inside and outside the probe. For the sample seen by the spectrometer to be representative of the plume at the skimmer entrance, the molecular beam must be undisturbed by surface or surface-induced scattering. Consequently, cryogenic pumping is a requirement as shown in Fig. 1. It has been shown (Ref. 1) that background scattering inside the probe is negligible if the probe pressure is maintained in or below the low 10^{-7} torr range. The probe thus is a molecular beam generator, designed so that the beam is representative of the exhaust plume chemical and gas dynamic state. This assumes that the flow is frozen at, or before, the skimmer aperture. The probe is applicable in the rarefied portions of the plume where skimmer effects may be neglected. The influence of the skimmer upon the plume flow field and the gas sample of the probe is minimized by partial pumping using liquid nitrogen (LN_2) on the external surfaces. External probe and chamber wall effects (chamber background) are treated extensively elsewhere (Refs. 1 and 2).

2.2 GAS SPECIES CONCENTRATION MEASUREMENTS

In addition to the beam scattering effect discussed above, the background gas can affect the spectrometer output signal when read directly. This is particularly true when the probe pressure becomes too high ($> 10^{-7}$ torr). The signal output is comprised of the background and beam gas components taken collectively. A true indication of the concentration of any given gas species at the sampling point can only be obtained if the probe background component is insignificant compared to or separated from the beam component. The latter may be accomplished by an A-C detection system. The beam is modulated with a mechanical chopper and read out with a lock-in amplifier referenced to the chopper rotational speed. The only portion of the gas stream that is detected is the portion which traverses along the probe centerline through the chopper wheel and into the spectrometer. The lock-in amplifier is only sensitive to A-C components of the proper frequency and phase. To account for any significant velocity difference existing between species of different mass, the beam flight distance should be as short as possible for essentially zero phase shift between chopping and detection.

With these provisions, the probe configuration is schematically shown in Fig. 2. The chopper wheel for this application should have 50-percent transmission as shown. Amplifier synchronization (reference) in the present configuration is by means of an electric lamp and photocell located directly opposite each other and 180 deg removed from the point of intersection of the beam and the chopper.

Typical exhaust gases of common fuels such as unsymmetrical dimethylhydrazine (UDMH)/N_2O_4 or MMH/N_2O_4 are water (H_2O), nitrogen (N_2), carbon monoxide (CO), hydrogen (H_2), and carbon dioxide (CO_2). Therefore, at least five major gas species from 2 to 44 amu must be sampled. Considerable sampling time may be saved if provision is made for scanning the selected gases rather than the entire mass spectrum. Figure 3 is the block diagram of a typical quadrupole mass spectrometer (M/S). Normal mass selection is provided by the ramp generator. Selective mass sampling is provided by substituting a stairstep control input, with each plateau corresponding to an assigned mass number.

Figure 4 is a block diagram of a mass switching system. Basically, the system consists of multivibrator circuits which select a given potentiometer and a given input to an OR logic circuit. All inputs are -10 v unless selected. The selected input is gated "on" because it is more positive than any other. The selected mass number is a function of the respective potentiometer setting. Provisions are made for a manual start or synchronization with external devices; stepping at a manual rate, internal selectable rate, or from a synchronized external source; and manual or automatic mass selection for setup or run conditions. During rocket firings, control and switching circuits cycle a given stepping sequence to correspond to the mass spectrum of interest. If the A-C detection scheme is used, this stepping rate must be compatible with the chopping speed and the filter time constant of the lock-in amplifier. For fast transient measurements, a 24,000-rpm motor and chopper with many peripheral blades would be required. Filter time constants down to 1 msec are typical of lock-in amplifiers. Fig. 5 shows the relationship between the spectrometer output and the mass switching control function.

2.3 VELOCITY DISTRIBUTION MEASUREMENTS

The basic probe configuration may be used to make velocity distribution measurements. Earlier discussions described how the probe was used to make steady-state measurements. The system for studying velocity distributions of the plume expansion is contrasted by its

transient measurements. It utilizes the time-of-flight technique and, again, is an adaptation of molecular beam techniques where the probe serves the purpose of molecular beam generator (Refs. 3 through 6). Figure 6 shows the probe configuration for velocity distribution measurements. The principle of operation is as follows. The beam passes through the slits of the chopper wheel giving an approximate impulse function of molecules. As time elapses, these molecules spread according to their respective velocities. Their arrival time at the detector ion source is inversely related to the velocity. Thus, the spectrometer output is a time-dependent function of the local density in the ion source.

The chopper wheel dimensions and number and width of slots depend on the relative flight time, beam diameter, dimensions of ionization region, and desired data acquisition time. The basic criterion is that the chopper aperture time is short compared to the molecular flight time. The chopper is driven by a small, two-phase, 400-Hz, 115-v, 24,000-rpm motor with a vacuum rating. A tunable oscillator was used for chopper speed control. A light and sensor were mounted directly opposite the beam and served as a timing reference and also for synchronization of the Waveform Eductor®.

The output of the ion source depends upon the density of all the background gas as well as the test gas. However, with a mass spectrometer tuned for the transmission of only the test gas, the major constituents of the ion source output are essentially rejected. The background "test" gas appears as random noise at the detector output since it has no coherent components with the frequency of the chopper wheel. These random components are removed by the eductor after preamplification, but those signals coherent with chopper rotation are retained. This includes the time-of-flight distribution as well as the stray signals from the motor drive circuits or induced by vibration. To establish a precise reference for time zero, the system must not be sensitive to chopper rotational direction; that is, adequate alignment requires that the beam aperture and light aperture to the synchronizing sensor be fully open at the same time.

Figure 7 is a basic block diagram of the eductor. The signal consisting of the distribution function plus the noise of the background gas may be amplified further at the eductor input. This composite signal is fed through one of several resistors onto a signal bus common to a bank of 100 memory capacitors. These capacitors are each connected to the signal bus through an insulated-gate field effect transistor. A precisely timed internal clock oscillator, which is externally started by the chopper synchronizing pulse, advances a ring counter which controls the memory gates. These gates close and open consecutively and

each of the memory capacitors in turn is tied to the signal bus. Since the sweeps are synchronized with the chopper rotation and the flight time of the gated molecular beam, the distribution is gradually stored in the memory. The same portion of the distribution function is applied to any given capacitor on successive sweeps. Because the signal is being integrated as a result of the selected time constant, the noise is suppressed. The capacitors are also connected to a high input impedance amplifier for isolation from the output terminations. Provision is made for "erasing" the memory and for "delayed" nondestructive readout of the memory at speeds completely independent of those used to store the waveform. Three output devices are used: (1) oscilloscope to observe status of data acquisition, (2) X-Y recorder for permanent record, and (3) data logger for entry into computer for data reduction purposes.

The time-of-flight mode has the greatest influence upon the physical configuration of the probe assembly. In particular, (1) the length of the probe is large to accommodate the required flight distance of the velocity mode, (2) the liquid-helium (LHe) reservoir must be ahead of the chopper wheel to avoid background gas scattering back into the molecular beam, and (3) the quadrupole head must be offset 90 deg so that the ion source will be in a fly-through configuration to ensure instantaneous density measurements. Item 2 above is significant since the chopper wheel is closed 98 percent of the time. As a result, cryogenic pumping is required in the probe for all plume constituents to maintain the pressure below 10^{-7} torr, thus eliminating "high" pressures between skimmer and chopper wheel. Item 3 also assures less contamination from reactive plume constituents and localized "high" pressures in the quadrupole tube.

2.4 TEST CHAMBER

An aspect that should not be overlooked in the discussion of the technique is the relationship of the test chamber performance to the probe performance. An obvious requirement is that the altitude simulation must be equivalent to orbital or near-orbital conditions (10^{-4} torr or less). If the chamber background pressure is not sufficiently low, the probe cryogenic pumps are subject to overload and a corresponding reduction in pumping speed. This in turn can introduce beam scattering problems and result in deterioration of the probe performance — ultimately affecting the quality of the data.

A chamber to meet this criterion requires cryogenic pumping of the exhaust products and also must maintain high vacuum conditions between firings. Such a chamber is described in later sections of this report.

Alternate chamber configurations could provide for pulse-mode firings and/or design of a rapid valving arrangement in the skimmer of the probe. Improvements in the technique to accommodate other chamber configurations are also discussed in later sections of the report.

SECTION III
DETAILED DESIGN AND OPERATIONAL FEATURES OF THE PROBE

The preceding section described the basic techniques used to make plume species density and velocity measurements. It is the purpose of this section to describe the physical features of the probe and to present some of the practical aspects of the measurements. Such things as sample pumping, beam chopping, probe mode changes, special mass spectrometer features, and probe alignment are particularly important.

3.1 BASIC PROBE ASSEMBLY

A probe assembly similar to Fig. 1 provides both internal and external surface pumping; LHe and LN_2 are required for this purpose. The LN_2 external surface pumping is used to minimize molecular backscatter and plume interference for about 50 percent of the gas components (H_2O and CO_2, among others). The reservoir for this function serves also as a radiation shield for the internal LHe pump. The LN_2 surfaces also provide additional pumping in the rear section of the probe. The LHe is required for H_2, N_2, CO, and nitrogen oxide (NO), among others, and the LHe reservoir is located between the skimmer and chopper wheel. All these features are shown in Fig. 8. Diffusion pumping was also felt necessary to pump residual H_2 and possible N_2 and He leakage that might originate from the probe or test chamber. A transition elbow is required for vertical mounting of the probe.

As indicated earlier, two different flight distances are required for velocity and density modes. The dimension of the flight distance and the chopper wheel for the velocity mode determine the basic dimension of the probe. The port (Fig. 6) closest to the skimmer is used for the chopper assembly in the velocity mode. In this configuration the rear port contains an ion gage for monitoring the probe internal pressure. An essential function of this ion gage is to provide a pressure interlock for the mass spectrometer head in case the probe pressure becomes too high. The two flange assemblies are interchanged at these ports with a velocity-density mode transition.

The LHe reservoir must be located between the skimmer and the chopper wheel in the velocity distribution mode. The chopper is closed for approximately 98 percent of the time so that with the LHe located elsewhere, the gas molecules reflected by the chopper become potential scattering elements for the incoming beam. This is not as much a problem for the density mode because of the different chopper design and location.

Since the probe walls are at LN_2 temperatures, care must be taken to ensure that the skimmer tip does not get too cold. The skimmer orifice was 0.040 in. in diameter and could conceivably become "plugged" if cooled to 77°K. Therefore the skimmer was shim stock which was fashioned into a cone and secured to a plexiglass truncated cone. This assembly in turn was threaded for mounting on the front of the probe.

3.2 CHOPPER ASSEMBLY

The important features of the chopper wheel are dictated for the most part by the velocity measurements. Aperture times for the current probe configuration are less than 15 μsec. The basic criterion is that the aperture time should be much less than the beam flight time after chopping. These considerations and others are thoroughly covered in the literature (Refs. 3 through 6). There are practical considerations which limit the length of the flight distance; the aperture time must be determined by beam cross section, chopper diameter, and rotational speed. Other considerations include the number of slots, desired data acquisition time, and signal-to-noise ratios. The following chopper specifications were used in the current experiments.

1. diameter - 4 in.
2. slots - 4
3. slit width - 0.060 in.
4. rotational speed - to 450 rps, nominal 400 rps
5. material - stainless steel
6. thickness - 0.001 in.

Items 5 and 6 are required because of the high rotational speed and limitation on flange size. Because of the small mass involved, vibration (and associated synchronous noise problems) is eliminated even at these high rotational speeds. Chopper insertion into the probe requires only folding the wheel back to fit flange dimensions. As the chopper rotates, centrifugal force straightens the wheel with minimum rubbing of nearby motor assembly components.

For the modulated beam density measurements, many of the same features are applicable. The significant difference is that 50-percent transmission is required. For lock-in amplifier considerations of response time, a high chopping rate is useful. The following specifications apply:

1. material - 0.001-in.-thick shim stock
2. circular openings - 12
3. rotational speed - to 400 rps
4. diameter - 4.25 in.
5. apertures - 0.469 on 1.8125 radius

The chopper assembly for this configuration is the rear flange to minimize the flight distance (zero phase difference) between chopper and quadrupole ionizer. The probe assembly end views of Figs. 2 and 6 show these general features of the chopper wheels.

A photocell was used as a detector for synchronization of the lock-in amplifiers and waveform eductor. Also, it is required to mark the reference time zero for the velocity time-of-flight measurements. For this purpose the timing pulse must have a rapid rise time with its peak properly aligned with the beam shutter function. As a consequence of the rise time, the photocell must be loaded heavily, resulting in a low pulse height. A preamplifier is therefore required in the motor assembly. Provision for temperature control of this amplifier and the motor is required. The chopper assembly was in thermal contact with LN_2 surfaces and required heaters and thermostats to ensure reliable operation.

3.3 SPECTROMETER HEAD ASSEMBLY

Several aspects of the spectrometer tube are of particular concern and require modification for this unusual configuration. The location of the head and the plume environment requires special consideration in the use of the spectrometer.

3.3.1 Ion Source

Shown in Fig. 9 is a drawing of the particular ion source used. Shown also is the relative orientation of the ion source with respect to the beam. The fly-through orientation is required for velocity measurements to remove any scattering surfaces from the beam cross section. A collimator is generally used ahead of the source. Even though scattering surfaces in the critical region of the source could be

removed with the alternate axial orientation of the head, this configuration was felt to be unadvisable because of the contaminating plume constituents that would be directed into the electron multiplier and quadrupole section of the head. Also, the right-angle orientation permits easy alignment with the centerline. A remotely operated valve on probe centerline permits unobstructed line of sight through the probe into the throat of the rocket.

3.3.2 Instrumentation Electrical Cable Length

One consideration that must be given to the mass spectrometer is its operation with extended line length. Standard cable lengths for most applications are approximately 10 ft, considerably less than that required for plume chamber installations. Conventional installations usually resolve H (1 amu) as the lowest detectable mass number. Because of the radio-frequency (RF) potentials required, extended cables in current commercial designs shift the operating frequency to a lower value until the lowest detectable mass number is considerably greater than that of H_2 (2 amu). For all fuels, hydrogen is one of the major exhaust constituents and is therefore of considerable interest in plume tests. Cable selection and cable routing must be chosen to minimize the capacitance loading on the RF tank circuits.

3.3.3 Input Amplifier

Essential to the operation of the system is the use of some type of buffer between the spectrometer multiplier output and the coaxial cable. In the interest of sensitivity, the multiplier load impedence must be large. However, this is not compatible with the capacitive loading as a result of cable shielding and the required overall frequency response of the system. In the present application a field effect input transistorized operational amplifier circuit was used and is shown in Fig. 10. The requirements of high amplifier input impedance for good signal levels at the multiplier output and low source impedance for driving coaxial lines are met with this device. This circuit is mounted directly on the quadrupole tube inside the probe. Because of the potentially cold environment, the amplifier must be warmed to maintain proper operating temperature. This temperature is maintained by a room temperature thermostat controlling an expended 40-w soldering iron element running at 3 w.

Consideration must be given to the isolation of the high voltage section of the multiplier/amplifier assembly to avoid serious arcing problems. During cycling of the thermostat an outgassing load may result from the heater system. The amplifier must be vacuum-isolated

from the multiplier, and adequate conductance for outgassing (or a good seal) must be provided.

3.4 PROBE ALIGNMENT

There are essentially two alignment problems that must be considered: alignment of (1) the probe beam with the exhaust plume streamlines and (2) the synchronizing pulse detectors with the probe beam. The system discussed here includes features for alignment at the time of installation.

3.4.1 Flow-Field Alignment

Provisions for probe alignment are required for (1) correction in misalignment attributable to thermal and structural contraction after chamber pumpdown and (2) flow-field alignment for off-axis sampling. The complete sampling of the flow field for plume mapping purposes requires a rather complex scanning mechanism. With a fixed nozzle position, three linear independent scanning actuators would be required for probe movement and two rotational actuators for flow-field alignment. Since the purpose of this test was for instrument evaluation, a much simpler approach was chosen for the installation. A fixed rocket probe separation distance and angular rocket nozzle positioning was used. The assumptions are that the expansion from the thruster appears as a point source which does not change with angular rotation. This point source was assumed to be at the center of the exit plane, and the vertical coordinate of the nozzle exit was chosen as the axis of engine rotation.

The centerline axis is established by the spectrometer ion source, skimmer tip, and the rocket nozzle centerline. To assure the alignment of these items, a laser beam was projected through an opening in the rear of the probe onto a target at the nozzle exit plane. A plexiglass skimmer was used to aid in alignment through the skimmer. The final installation and adjustments, discussed in the next section, require compensation for probe and nozzle movement after pumpdown. These are principally attributable to cryogenic thermal effects rather than chamber loading under vacuum conditions.

3.4.2 Synchronizing Pulse Timing Alignment

Accurate velocity measurements require the synchronizing pulse to occur at the exact instant of the slit opening. The synchronizing detector sensitive area should be the same width as the effective beam diameter

at the chopper location so the synchronizing pulse would be essentially a duplication of the shutter function.

Adjustments in synchronizing alignment are made with the laser arrangement described in the preceding discussion. Shown in Fig. 11 are the significant features of the alignment procedure. With a laser beam projecting along the probe centerline, another photodetector is located at the skimmer opening. The three possible conditions for the occurrence of the two pulses are shown. Obviously condition "b" is appropriate. This condition is obtained by lateral adjustments of the motor assembly. Frequently the accuracies of the chopper fabrication with regard to slit location required adjustment as shown in "e." Typically, this amounts to a 3-μsec error for rotational speeds of 400 rps.

Symmetry in the probe design was maintained as much as possible to limit any movement of the motor assembly with respect to the spectrometer ionizer. In particular the flanges were made small and diagonally opposite except for the velocity motor assembly flange. Misalignment attributable to cryogenic contractions during cooldown is thereby minimized.

3.5 CRITERIA FOR SELECTION OF PROBE PHYSICAL DIMENSIONS

Selection of dimensional features of the probe requires consideration of several interrelated effects. The probe physical dimensions necessarily must finally be selected on the basis of whether they are practically feasible. The flight distance and beam cross section also are not independent selections.

Effects that must be considered for flight distance selection are

1. practical physical length of probe as determined also by
   a. skimmer
   b. pump sizing and transition elbow (vertical mounting)
2. anticipated plume gas velocities
3. allowable width of shutter function (Refs. 3 and 4)
4. dimension of ionization region
5. electronics response time (Ref. 3)

A general criterion is that the flight time must be long compared to shutter function, ion source transmission time, and electronic response time.

Effects that must be considered for beam cross section selection are

1. shutter function width
2. skimmer orifice size
    a. probe gas load from chamber background and thruster
    b. anticipated pressure rise
    c. detector sensitivity
3. entrance aperture to spectrometer ion source
4. flight distance
5. chopper-skimmer orifice separation

Because of the excellent pumping capabilities of the probe and rather inflexible geometry of the ion source, item 1 is the most significant consideration.

Probe diameter for a symmetrical design is determined principally by the chopper wheel diameter. Twice the chopper diameter is a minimum dimension without resorting to such features as canted wheels with respect to probe centerline.

The skimmer length is determined principally by the probe diameter as discussed above and gas dynamic consideration related to the proper angle to ensure external attached oblique shocks and no internal shocks in the skimmer. This relatively long dimension provides a rather large internal volume for liquid helium storage, minimizing the number of refills and associated losses.

SECTION IV
EXPERIMENTAL APPARATUS AND TYPICAL PROBE AND SYSTEM PERFORMANCE

4.1 TEST FACILITY

The test was conducted in the Aerospace Research Chamber (10V) of the Aerospace Division of the von Kármán Gas Dynamics Facility (VKF). A sketch of the chamber is shown in Fig. 12. The stainless steel chamber is 20 ft long and 10 ft in diameter. The cryopumping surfaces designed for removing exhaust products from rocket engines were arranged to optimize the heat load distribution such that it would be compatible with the capacity of the refrigeration systems. Since the

operation of the probe is intended for far-field applications, its performance can be influenced by the chamber performance. The particular configuration of the chamber cryosurfaces is compatible by minimizing backscatter from the walls and maintaining a low ($<10^{-4}$) background.

The sketch of Fig. 13 shows the arrangement of the cryosurfaces to pump the high enthalpy exhaust gas products. The gas leaving the engine passes through the radially arranged GHe surfaces and impinges on the annular LN_2 cryosurface where most of its total energy is removed. The cooled gas is then either cryopumped by the LN_2 surface or reflected onto the GHe cryosurface where it is condensed. There is a total GHe refrigeration capacity of 8 kw. Since H_2 has a high vapor pressure (10^{-4} torr) on 15°K GHe surfaces, LHe (4.2°K) was used to remove the H_2. The H_2 exhaust gas moves axially down the chamber, impinges on the LN_2 cryosurfaces where energy is removed, and then is cryopumped on the LHe cryosurfaces. The LHe required for pumping H_2 was transferred from a 500-liter dewar located at the side of the chamber.

4.2 TEST INSTALLATION

The test installation included provision for a source of known flow conditions in addition to the rocket. The known source was a heated sonic orifice and the rocket was a 1-lb MMH/N_2O_4 thruster. The heated orifice proved invaluable for checkout purposes and to verify the system performance, particularly in the velocity mode.

The probe installation is shown in Fig. 14. The particular configuration shown is for alignment purposes. A vacuum-rated valve at the rear of the probe is opened for projecting a laser beam along the probe centerline. A plexiglass skimmer is used to aid in alignment. The laser is then projected to the source by alignment of the source and/or the probe. The several chamber cryogenic pumping systems described above may also be seen.

The installation for the sonic orifice is shown in Fig. 15. The orifice was a 0.040-in.-diam hole in a thin-wall tungsten tube. This tube also served as a heating element, and source temperatures in excess of 2000°K could readily be obtained. The source was mounted on a scanner so that in later stages of the test program the sources could be interchanged. The scanner positioning also could provide for variable axial source-skimmer separation distances.

The installation for the thruster is shown in Fig. 16. A linear actuator (not shown) was provided to rotate the thruster about the exit plane of the nozzle. Rotation from 0 to 27.5 deg was possible for studying spatial effects of the exhaust plume. The separation distance for the investigation was fixed at 35 nozzle exit diameters.

4.3 ROCKET ENGINE

The 1-lb scaled thruster used in the test was supplied by McDonnell Douglas. The bipropellant MMH/N_2O_4 thruster was designed for both steady and pulsing operation. The performance of the engine was investigated by Marquardt Corporation personnel who found that the smaller thrust level resulted in lower combustion efficiency and pulsing performance. During the firing, the propellant valves and injectors were held at 60°F with cooling water.

The thruster design parameters and performance are shown below.

Thrust	1.0 lb
Fuel	MMH
Oxidizer	N_2O_4
Chamber Pressure	90 psi
Mixture Ratio	1.65 ± 0.15
Nozzle Expansion Ratio	40:1
Nozzle Geometry	Contoured
Chamber Temperature	4000°F
Throat Diameter	0.090 in.
Nozzle Exit Diameter	0.569 in.
Combustion Efficiency	0.830

The low combustion efficiency is substantiated by measurements discussed in a later section of the report. The actual measured contour of the nozzle is shown in Fig. 17 and Table I (Appendix III). Shown in Fig. 18 is the assembled 1-lb thruster. It consists of a single-doublet water-cooled injector head, high response solenoid valves, and two 5-micron nominal filters upstream of each valve. The nozzle and combustion chamber are an integral part, machined from molybdenum.

The 1-lb thruster propellant system consists mainly of three parts: the engine nitrogen purge, high-point bleeds, and propellant supply system. Each propellant tank has a capacity of 2 liters and was pressurized with dry nitrogen. The arrangement used made it possible to run cold gases for system checkout purposes, thus avoiding the necessity of running the engine unnecessarily.

4.4 TECHNIQUE AND SYSTEM PERFORMANCE EVALUATION USING A SONIC ORIFICE SOURCE

The modulated beam technique discussed earlier in the report and used in this probe is an accepted instrumentation technique in molecular beam systems. For compatibility with rocket plume testing the usual features must be modified. Significant among these is response time which in general must be fast enough to limit the engine firing time or for pulse mode testing. This response time criterion applies for both the density and velocity modes and is discussed below.

4.4.1 Exhaust Species Relative Density Measurements

The modulated beam technique and its performance has been described elsewhere (Ref. 7). However, the current application requires a chopping rate generally greater than other beam applications; this may be seen from the following discussion. If a mass scan from H_2(2) through NO_2 (46) is required every second, this would give approximately a 0.02-sec/amu sweep rate. Assuming for the sake of discussion that the individual species come through as symmetrical triangles, it would require a filter time constant of no more than 0.1 msec for the lock-in amplifier to follow the input to within 1 percent. This is for a 6-db/octave rolloff and an equivalent bandwidth of 1600 Hz (3 db). Very little noise reduction would result with such a small time constant. Also, a rather high chopping rate would be required for adequate filtering of the synchronous frequency. Thus, little would be gained by using the lock-in amplifier. Generally, a 1-msec time constant is the minimum selection available anyway.

The alternate consideration involves the application of mass switching the spectrometer. There are seven major mass peaks of interest. If these are to be collectively sampled at 1-sec intervals, and allowing 4.6 time constants so that 99 percent of final value may be reached after switching, a 30-msec time constant results. This technique is shown in Fig. 5. This time constant gives a filter bandwidth of approximately 5 Hz and a synchronous reduction factor of at least 40 db if a chopping frequency greater than 500 Hz is used.

A 12-aperture chopper is currently used with a 400-rps motor, resulting in a maximum chopping speed of 4800 Hz. A 40-db synchronous reduction factor requires a time constant of 6.5 msec such that 30 msec/specie mass stepping rate is feasible and yields a spectrum sampling interval of approximately 0.2 sec. These criteria are of course not considering the noise/signal component which is determined by the probe background pressure.

The effect of background noise and the characteristics of the detector system when using discrete specie sampling may be seen in Fig. 19. The experiment involved a three-component mixture of typical species expanding from a sonic orifice. These measurements were made in a calibration chamber and involved only the instrumentation devices without the probe assembly. The background pressures were in the low 10^{-6} torr range with the larger percentage being H_2. These were centerline measurements such that no H_2 was observed because of mass separation effects; H_2 was observed in off-axis measurements. The effect of filter time constant is obvious when considering both rise time and noise. It should be indicated, however, that the use of beam modulation is necessary only for situations where the background gases are significant. In this respect, the plume chamber environment and pumping capacity are closely related to the instrumentation technique used. It will be shown later that the probe used in these experiments was able to maintain a low enough background pressure for direct reading without beam modulation.

4.4.2 Velocity Distribution Measurements

The calibration system used in the experiments described above was also used to verify the performance of the technique for velocity measurements. Figure 20 is a typical oscilloscope waveform obtained. The first trace shows the output of the waveform eductor; the second, the spectrometer input before signal averaging. The need for waveform enhancement is obvious. The individual time segments represented by the charge on the 100 storage capacitors may be observed as a "staircase" at the eductor output. Most of the experiments were run in the range from 1 to 4 x 10^{-7} torr. The experiments involved in this evaluation were from a source at sufficient low pressure to ensure a Maxwellian distribution. By curve fitting the experimental data to a Maxwell-Boltzmann distribution, the temperature could be readily calculated. Figure 21 shows distributions obtained for a heated source for two different temperatures. A comparison with known theoretical Maxwellian can also be made. Reference time zero for the experimental results is indicated as t_o', whereas t_o is the reference time zero for the Maxwellian distribution. The interval between t_o and t_o' is the quadrupole flight time and is the time required between molecular ionization and detection, most of which is the drift time down the quadrupole section of the spectrometer (Ref. 3).

4.5 TECHNIQUE AND SYSTEM PERFORMANCE EVALUATION USING THRUSTER

The probe evaluation using the thruster was undertaken after having determined the basic performance using the sonic orifice. Of particular

interest was the determination of the performance of the pumping system and the adequacy and reliability of the data obtained. No attempt to analyze the data will be made here.

4.5.1 Probe Pressure Performance

It was indicated earlier in the report that the probe internal pressure is important to the extent that it can influence the data by contributing to the spectrometer background noise and to beam scattering effects. Shown in Fig. 22 is the pressure performance of the probe for a typical rocket firing. These data were taken after filling the probe LHe reservoir before engine firing. These data were taken with the probe in the velocity mode. No significant difference was observed for the density configuration. The probe pressure consistently remained on low 10^{-8} torr range during engine firing; a transition into the 10^{-7} torr region could reliably be interpreted as something wrong. Prime candidates were warming of the LHe reservoir or excessively high chamber pressure.

Shown in Fig. 23 is the Chamber 10V performance during thruster firing. Extended firings of 1 min or more usually resulted in higher pressures by approximately an order of magnitude. This response required the chamber LHe reservoir to be full and flowing LHe before engine firing. Indeed the success of the probe was due in part to the chamber maintaining such a hard vacuum during engine firings. If for some reason, malfunctional or operational, the chamber pressure went beyond 1 μ, it was generally immediately observable in the probe performance.

With the probe pressure in the 10^{-8} torr range, data acquisition was considerably simplified for both density and velocity measurements. These effects are discussed in later sections of the report.

4.5.2 Species Identification and Density Measurements

The typical results of a species identification experiment may be seen in Fig. 24. These results were obtained without beam modulation. The major plume constituents are clearly observable. Verification that indeed the spectrometer output was the beam rather than background gas and beam was made with sonic orifice checks having flow densities comparable to those produced by the thruster. The relative comparison of the output for beam off and on, as determined by the chopper wheel position, indicated that the mass spectrometer output was essentially zero when the beam was blocked. This was to be expected in view of low probe background pressure as discussed earlier.

The spectrum in Fig. 24 is from C (12) through NO_2 (46). The species indicated are those which are not ambiguous. For comparison, Table II shows the constituents for MMH/N_2O_4 with an O/F ratio of 1.6. These results are theoretical and are for chemical equilibrium. As shown later, however, the combustion processes for this system are less than ideal, and these values should be taken with some reservations (Ref. 8).

4.5.3 Velocity Distribution Measurements

Shown in Fig. 25 is a typical time-of-flight measurement. This distribution was obtained for the N_2/CO mass peak on the centerline of the thruster and plume. Shown as an insert is the time-of-flight measurement before signal averaging. Although the distribution is not symmetrical, as a first approximation the most probable flight time may be used to determine the mean velocity. It will be shown that this can be used to relate velocity to the source temperature. The calculated mean velocity is approximately equivalent to a 2100°K source. This is comparable to 2500°K calculated temperature for the combustion process. Although not conclusive, this comparison lends some confidence to the results. Another aspect of the distribution function is its shape. The width of the distribution was considerably greater than anticipated. Previous results using expansion of heated single species or simple mixtures indicated speed ratios much greater than experienced for the thruster. However, it can be shown that by virtue of the peculiarities of the thruster and nozzle, the low speed ratios are not unreasonable. Such considerations are discussed more thoroughly in the next section.

SECTION V
RESULTS AND DISCUSSION
OF CHEMICAL AND GAS DYNAMIC MEASUREMENTS

A discussion of the chemical and gas dynamic properties of an expansion process as complicated as a rocket exhaust cannot be covered completely here. The object of the test was to establish the feasibility of instrumentation techniques. The chemical and gas dynamic properties to be discussed are merely byproducts of the test effort. However, some observations concerning the chemical and gas dynamic properties are presented for comparison to theoretical results. The departure of these properties from the conventional concepts and analysis is discussed. Some of the experimental results are thought to be attributed to the characteristics of the particular thruster used and may or may not be typical of larger rockets of more conventional design.

5.1 RELATIVE GAS DENSITY MEASUREMENTS

The time required for a complete and adequate calibration so that absolute number densities could be obtained was not available for this test. However, certain relative effects may be observed. The apparent discrepancy between Table I and Fig. 24 may in part be attributable to the sensitivity of the spectrometer to the various constituents, but it is too significant to be explained completely in this way. The N_2/CO peak is the most significant mass peak. The most notable difference, however, is O_2, NO, and NO_2. This aspect substantiates the rather poor efficiency and the incomplete combustion process mentioned earlier. Related also to this is the rather low water peak. Interpretation of the water peak is difficult since H_2 was not among the sampled species. Because of the long RF lines required, H_2 could not be detected in this installation. Mass separation effects may have contributed also to the lack of hydrogen. The H_2O could be low if the H_2 peak is significant or attributable to low spectrometer sensitivity in this mass range.

Mass numbers 12 through 17 require some interpretation because of spectrometer cracking patterns. Multiple contributions to the output signal are a result of double ionization or dissociation of heavier species. For example, mass 14 peak can come from (a) N_2^{++}, (b) CO^{++}, or (c) N_2, NO, NO_2 dissociated species. The dissociation may thus be a result of the spectrometer or the actual combustion process in the thruster. Secondary peaks caused by spectrometer cracking patterns may be as high as 10 to 12 percent of primary peak.

The mass range from 12 to 17 also has primary constituents as a result of the combustion process. Significant among these are methane and ammonia. The following list summarizes the possible constituents of the 12 to 17 range.

Mass No.	Primary Constituents	Dissociation	Double Ionization
12	C	CO, CO_2	---
13	---	---	---
14	N	N_2, NO, NO_2	N_2, CO
15	---	---	NO
16	CH_4, O	O_2, CO, CO_2	O_2
17	NH_3, OH	H_2O	---

It appears obvious from this tabulation that little or no significance may be attached to this mass range.

One experiment involved making a series of relative density measurements off centerline by rotating the thruster up to 27.5 deg. The data are shown for the N_2/CO peak in Fig. 26. For comparison purposes, the theoretical mass flow is also shown assuming free expansion without bounds. This comparison requires normalization to centerline values. The experimental results indicates the deviation begins at 22 deg. Other major species respond similarly. Another effect is the appearance of species 26, 27, 29, and 39 at the larger angles. This is also thought to be a boundary or wall effect. However, it is interesting to note that reactive components NO_2 and O_2 decreased much faster as the plume became more rarefied — to the extent of being nondetectable at large angles.

Of interest also is how the mass spectrum changes with O/F ratios. Figure 27 shows the mass spectrum at shutdown for an O/F ratio of 1.9. The most notable feature is the extreme NO_2 and NO peaks with respect to N_2 and H_2O. The range from 40 to 46 is significantly different when compared to a nominal 1.6 O/F ratio. Visual observations during this and similar off-specification firings noted that a heavy green contamination was deposited on the external probe cryosurfaces. The particular significance of these experiments is the potential of the sampling technique for optimizing thruster specifications.

5.2 VELOCITY DISTRIBUTION MEASUREMENTS

Numerous analyses of the data reduction of molecular time-of-flight measurements have been reported (Refs. 5 and 9 to 13). Basically these data reduction techniques assumed the form of the molecular distribution function to be Maxwellian. (In addition to the Maxwellian distribution function, Amend (Ref. 5) has also considered the ellipsoidal and perturbed ellipsoidal distribution functions.) This functional form was related to the measured signal S(t), which is proportional to the number of molecules in the ionization region at an instant of time (assuming ionization is infinitely fast). Then an appropriate fitting (Ref. 13) was made between the measured signal, S(t), and its relation to the assumed form of the distribution function in order to determine the speed ratio and mean translational temperature.

The Maxwellian distribution function is actually valid only for a monatomic gas in equilibrium or local translational equilibrium. It is unlikely that the exhaust of a rocket engine with chemical reactions taking place is in equilibrium. Also, even if chemical reactions in such a flow have ceased, the assumption of a Maxwellian distribution function cannot be valid since the flow is a mixture of gases of complex molecular

structure. Furthermore, it has been shown by Hamel and Willis (Ref. 14) and Edwards and Cheng (Ref. 15) that even a monatomic gas does not have a Maxwellian distribution function in a highly expanded flow, such as the far field of a plume. Therefore, with these uncertainties in mind concerning the distribution function, it seems inappropriate to assign a functional form to the distribution since it is, in fact, the purpose of the measurement and hence should be given full opportunity to describe the gas properties.

5.2.1 Data Reduction of Time-of-Flight Measurements

A derivation of the relationship between the measured signal, S(t), and the free-stream velocity distribution function, f(u), is given in Appendix II. The results of this derivation are repeated here for convenience as

$$t^2 S(t) \approx f(\ell/t) \tag{1}$$

where ℓ and t are the flight distance and time, respectively. Assuming that the transverse and parallel velocity components are independent, the mean free-stream velocity is

$$\bar{u} = \frac{\int_0^\infty u f(u)\, du}{\int_0^\infty f(u)\, du} = \frac{\int_0^\infty \frac{\ell S(t)}{t}\, dt}{\int_0^\infty S(t)\, dt} \tag{2}$$

and for the average of the square of the free-stream velocity

$$\overline{u^2} = \frac{\int_0^\infty u^2 f(u)\, du}{\int_0^\infty f(u)\, du} = \frac{\int_0^\infty \frac{\ell^2 S(t)}{t^2}\, dt}{\int_0^\infty S(t)\, dt} \tag{3}$$

The translational kinetic temperature, T, is defined by (Ref. 16)

$$\frac{3}{2} KT = \frac{1}{2} M \overline{\left[(u-\bar{u})^2 + (v-\bar{v})^2 + (w-\bar{w})^2\right]} \tag{4}$$

Considering the transverse and parallel velocity components, the temperature of Eq. (4) includes both $T_\parallel$ and $T_\perp$. With certain assumptions regarding the relative magnitude of $T_\parallel$ and $T_\perp$, and since only the u component of velocity has been measured, it is shown in Appendix II that

$$RT_\parallel = \frac{1}{3}\left[\overline{u^2} - (\bar{u})^2\right] \tag{5}$$

From the definition of speed ratio one obtains

$$S = \frac{\bar{u}}{\sqrt{2RT_{\parallel}}} = \frac{\bar{u}}{\left\{\frac{2}{3}\left[\overline{u^2} - (\bar{u})^2\right]\right\}^{1/2}} = \left\{\frac{2}{3}\left[\frac{u^2}{(\bar{u})^2} - 1\right]\right\}^{-1/2} \tag{6}$$

5.2.2 Results of Time-of-Flight Measurements

Measurements were made at $x/d_e = 35$ of the $A/A^* = 40$, contoured, 1-lb, MMH/N_2O_4 thruster. In addition to the MMH/N_2O_4 firings, cold flow CO_2 and N_2 runs were made using the thruster, and an Ar run was made using a sonic orifice. The measured signal S(t) versus time-of-flight data are presented in part (a) of Figs. 28 through 30 for the cold flow runs, and in part (a) of Figs. 31 through 34 for the N_2 constituent of the MMH/N_2O_4 firings. The resulting u component of the velocity distribution function is presented in part (b) of each of the Figs. 28 through 34. The value of u at which f(u) attains its maximum value in part (b) of Figs. 29 through 34 is the most probable velocity, U_{mp}. The mean velocity, $\bar{u}$, and square root of the mean of the velocities squared (root-mean-square velocity), $\sqrt{\overline{u^2}}$, were determined by numerically integrating the appropriate function of S(t) described in Eqs. (2) and (3). From $\bar{u}$ and $\sqrt{\overline{u^2}}$ other mean gas properties can be calculated as illustrated in the previous section by the calculation of $T_{\parallel}$ and $S_{\parallel}$.

The results presented in Figs. 28 through 30 for the cold flow gases illustrate that the speed ratio increases as the distribution function becomes more narrow. Of particular interest is that for CO_2 (Fig. 29) the velocity distribution is that which might be calculated for a free-jet expansion from the nozzle. That is, for CO_2, $\gamma = 1.28$, the speed ratio at 35 nozzle diameters is comparable to the expected speed ratio from an ideal MMH/N_2O_4 exhaust at the same location. An increase in $S_{\parallel}$ is shown in Eq. (6) to be caused by the ratio, $\overline{u^2}/(\bar{u})^2$, of the moments $\overline{u^2}$ and $(\bar{u})^2$ of the distribution function, decreasing to one. For these highly expanded, cold flow, single specie measurements, the total temperature can be approximated by using isentropic flow relations and neglecting the static temperature since nearly all the energy has been converted into organized motion. Therefore, for a perfect gas

$$T_o \approx \frac{(\bar{u})^2}{2\,c_p} = \frac{(\gamma-1)\,(\bar{u})^2}{2\gamma R} \tag{7}$$

The quality of this approximation depends upon the equilibrium state of the gas. Since nonequilibrium flow is a time-dependent process, one

would have to know the history of the gas from the reservoir to the point of measurement in the plume in order to calculate T_o accurately. Therefore, calculated values of T_o are presented only for the cold flow measurements by assuming γ to be constant, which of course is not strictly the case, particularly for the CO_2 expansion. No calculations of T_o are presented for measurements made in the rocket plume since this thruster is considered to have a highly nonequilibrium flow (which is common to small rocket engines).

Note the wide molecular velocity distributions of N_2 in the MMH/N_2O_4 firings in Figs. 31 through 34. The unexpectedly wide distribution produced large values of $T_{\parallel}$. In view of the resulting low speed ratios, the actual rocket contour was measured to ±0.001 in. and a characteristics solution was obtained to determine if a compression shock could be formed inside the nozzle causing the unusually large values of static temperature. The solution was obtained with a perfect gas approximation and $\gamma = 1.31$. The resulting characteristic network is shown in Fig. 35. Note in Fig. 35 that a compression shock is formed in the nozzle and propagates downstream. This solution is assumed to be representative of the actual flow from the rocket, and, if indeed it is, the shock propagated downstream of the nozzle exit could cause large values of $T_{\parallel}$ and decrease speed ratio $S_{\parallel}$. If a shock does not exist in the flow, then it is suspected that considerable afterburning may have taken place and thereby produced large static temperatures.

SECTION VI
SUMMARY AND CONCLUDING REMARKS

In the final evaluation tests, velocity and density distributions of molecular species were made in a 1-lb rocket exhaust plume at near-orbital altitudes. The following concluding observations may be made:

1. The probe pumping system is capable of maintaining high vacuum conditions (10^{-8} torr) for mass spectrometer operation.
2. Good instrument response time and sensitivity can be obtained.
3. The sensitivity was unaffected by considerable contamination introduced from the engine — the sensitivity was essentially stable during any series of runs.
4. Mass resolution was unaffected by the remote operation of the spectrometer head.

5. Typical mass spectrums of rocket exhaust constituents can be obtained and responded logically for variations in engine O/F ratios.
6. Density measurements can be made with or without beam signal modulation.
7. The measured most probable flight time agreed well with theory and corresponded to a velocity of 2000 m/sec.
8. The static temperatures obtained from velocity distribution were much greater than anticipated and was partially caused by incomplete combustion and nozzle shocks.
9. Data acquisition time for a single mass number velocity distribution was less than 3 sec.
10. Variations in velocity distribution for different mass species were small.

The most serious limitation of the system and data discussed here is the lack of an adequate and reliable calibration. This limitation in part has as its source the use of mass spectrometer and the quadrupole in particular. In the current test, partial solution of the calibration problems was undertaken by the use of known source conditions in a sonic orifice expansion. This may be used as a standard for number densities and sensitivity adjustments. However, overlapping peaks (N_2/CO in particular), no standard cracking pattern for quadrupole, and calibrating sources for species as H_2O and NO_2 still present no small problem. Therefore, other techniques are required to complement the measurements of the mass spectrometer probe discussed here.

With regard to the velocity measurements, the cold flow runs with CO_2, N_2, and Ar verified that the system could adequately measure velocity distributions and deduce, from the measurements, static temperatures as low at 1.9°K and speed ratios as high as 18. The measured velocity distribution of the rocket exhaust plume gas provided speed ratios of approximately 3.0 and static temperatures of 600°K. The low values of speed ratio and high values of static temperature were not in agreement with predicted speed ratios and temperatures. Analysis of the nozzle expansion indicated a developed bell compression shock which could alter the predicted expansion. For complete evaluation of the velocity distribution of the exhaust plume, a more detailed analysis of the shock system is required. Also, evaluations with thrusters of improved performance could be used to further establish the validity of the system.

REFERENCES

1. Benek, J. A. and Powell, H. M. "Investigation of Performance Parameters of a Mass Spectrometer Sampling Probe in Rarefied Flows." AEDC-TR-70-79 (AD707843), June 1970.

2. Muntz, E. P., Hamel, B. B., and Maguire, B. L. "Exhaust Plume Rarefaction." AIAA Paper No. 69-657, AIAA Fluid and Plasma Dynamics Conference, San Francisco, California, June 16-18, 1969.

3. Powell, H. M. and Heald, J. H., Jr. "A System for the Measurement of Velocity Distributions of Molecular Beams." Fourteenth National Vacuum Symposium, American Vacuum Society, October 1967.

4. Hagena, O. F., Varma, A. K. "Time-of-Flight Velocity Analysis of Atomic and Molecular Beam." Review of Scientific Instruments, Vol. 39, No. 1, January 1968, p. 47.

5. Amend, William E. "Application of Statistical Moments in the Reduction of Supersonic - Molecular - Beam Data." Report No. AS-68-4, University of California, Division of Aeronautical Sciences, June 1968.

6. Scott, P. B., Bauer, P. H., Wachman, H. V., and Trilling, L. "Velocity Distribution Measurements by a Sensitive Time-of-Flight Method." Fifth International Symposium on Rarefied Gas Dynamics, Vol. II, Academic Press, New York, 1967.

7. Heald, J. H., Jr. "The Performance of a Mass Spectrometric Modulated Beam Detector for Gas-Surface Interaction Measurements." Vacuum, Vol. 17, No. 9, September 1967, p. 511.

8. Muengen, J. R. and Griener, L. "Estimation of Performance Factors for Rocket Propellants." Texaco Experiment, Incorporated, 1962.

9. Kantrowitz, A. and Grey, J. "A High Intensity Source for the Molecular Beam, Part I, Theoretical." Review of Scientific Instruments, Vol. 22, No. 5, May 1951, pp. 328-332.

10. Parker, H. M., Kuhlthau, A. R., Zapata, R., and Scott, J. E., Jr. "The Application of Supersonic Beam Sources to Low-Density, High-Velocity Experimentation." Rarefied Gas Dynamics, edited by F. M. Devienne. Pergamon Press, Inc., New York, 1960, pp. 69-79.

11. Hagena, O. F. and Henkes. "Investigation of the Thermal Relaxation in Nozzle Flows by Analysis of the Gas Kinetic Velocity Distribution." Zeitschrift Fur Naturferschung, Vol. 15a, No. 10, October 1960, p. 851.

12. Anderson, J. B. and Fenn, J. B. "Velocity Distributions in Molecular Beams from Nozzle Sources." The Physics of Fluids, Vol. 8, No. 5, May 1965, pp. 780-787.

13. Wilmoth, R. G. and Hagena, O. F. "Scattering of Argon and Nitrogen Off Polycrystalline Nickel." University of Virginia Report No. AEEP-4038-105-67U, August 1967.

14. Hamel, B. B. and Willis, D. R. "Kinetic Theory of Source Flow Expansion with Application to the Free Jet." The Physics of Fluids, Vol. 9, No. 5, May 1966, pp. 829-841.

15. Edwards, R. H. and Cheng, H. K. "Steady Expansion of a Gas into a Vacuum." AIAA Journal, Vol. 4, No. 3, March 1966, pp. 558-561.

16. Chapman, S. and Cowling, T. G. The Mathematical Theory of Non-Uniform Gases. Third Edition, Cambridge University Press, Cambridge, 1970.

17. Edwards, R. H. and Cheng, H. K. "Distribution Function and Temperatures in a Monatomic Gas Under Steady Expansion into a Vacuum." Rarefied Gas Dynamics, Supplement 4, Vol. 1, Academic Press, New York, 1967, pp. 819-836.

18. Willis, D. R. and Hamel, B. B. "Non-Equilibrium Effects in Spherical Expansions of Polyatomic Gases and Gas Mixtures." Rarefied Gas Dynamics, Supplement 4, Vol. 1, Academic Press, New York, 1967, pp. 837-860.

19. Cooper, A. L. and Bienkowski, G. K. "An Asymptotic Theory for Steady Source Expansion of a Binary Gas Mixture." Rarefied Gas Dynamics, Supplement 4, Vol. 1, Academic Press, New York, 1967, pp. 861-879.

APPENDIXES

I. ILLUSTRATIONS
II. DEVELOPMENT OF EQUATION FOR ANALYSIS OF TIME-OF-FLIGHT MEASUREMENTS
III. TABLES

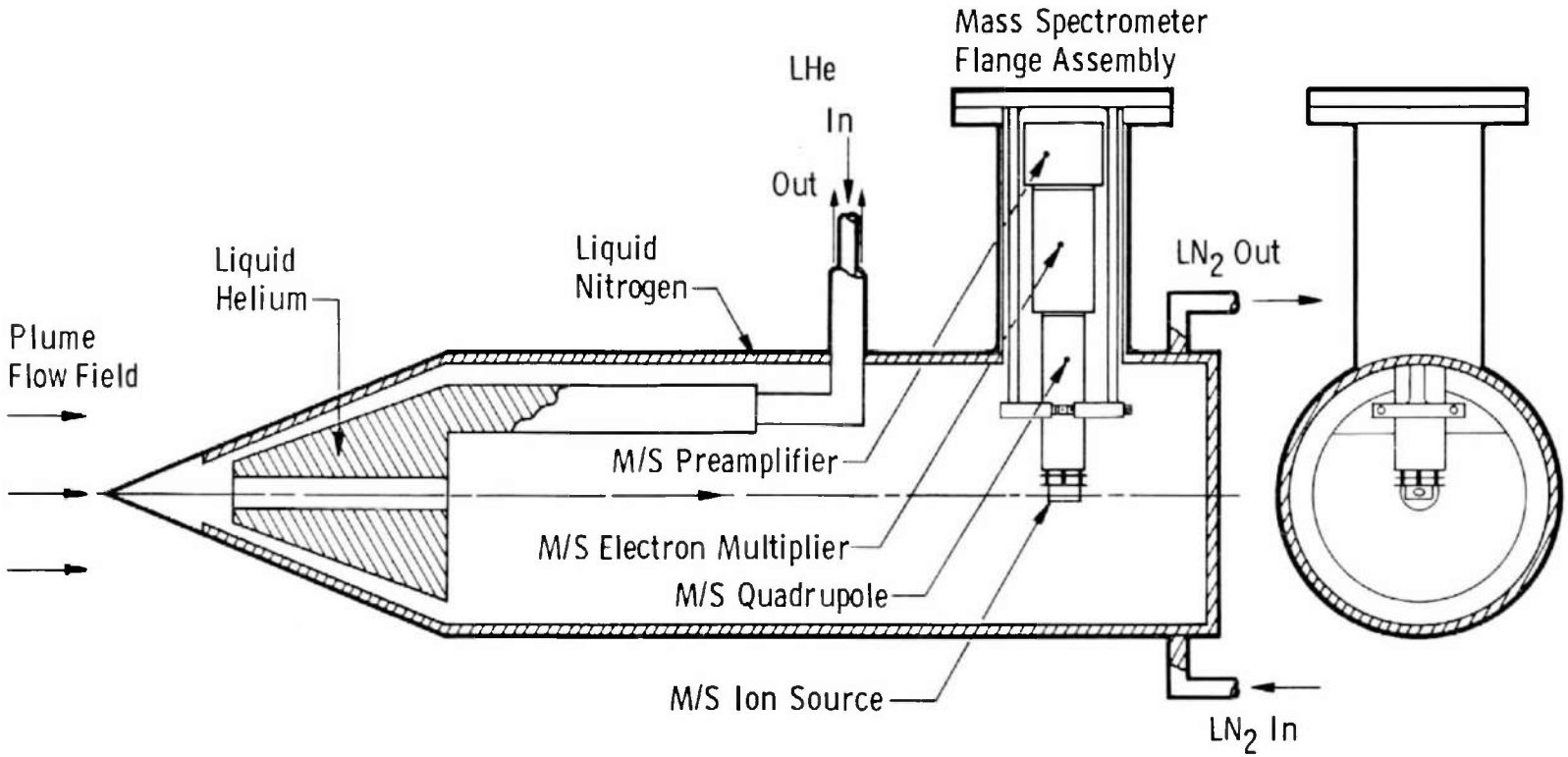

Fig. 1 Basic Probe Design Showing Mass Spectrometer Assembly and LHe/LN_2 Cryogenic Pumping Configuration

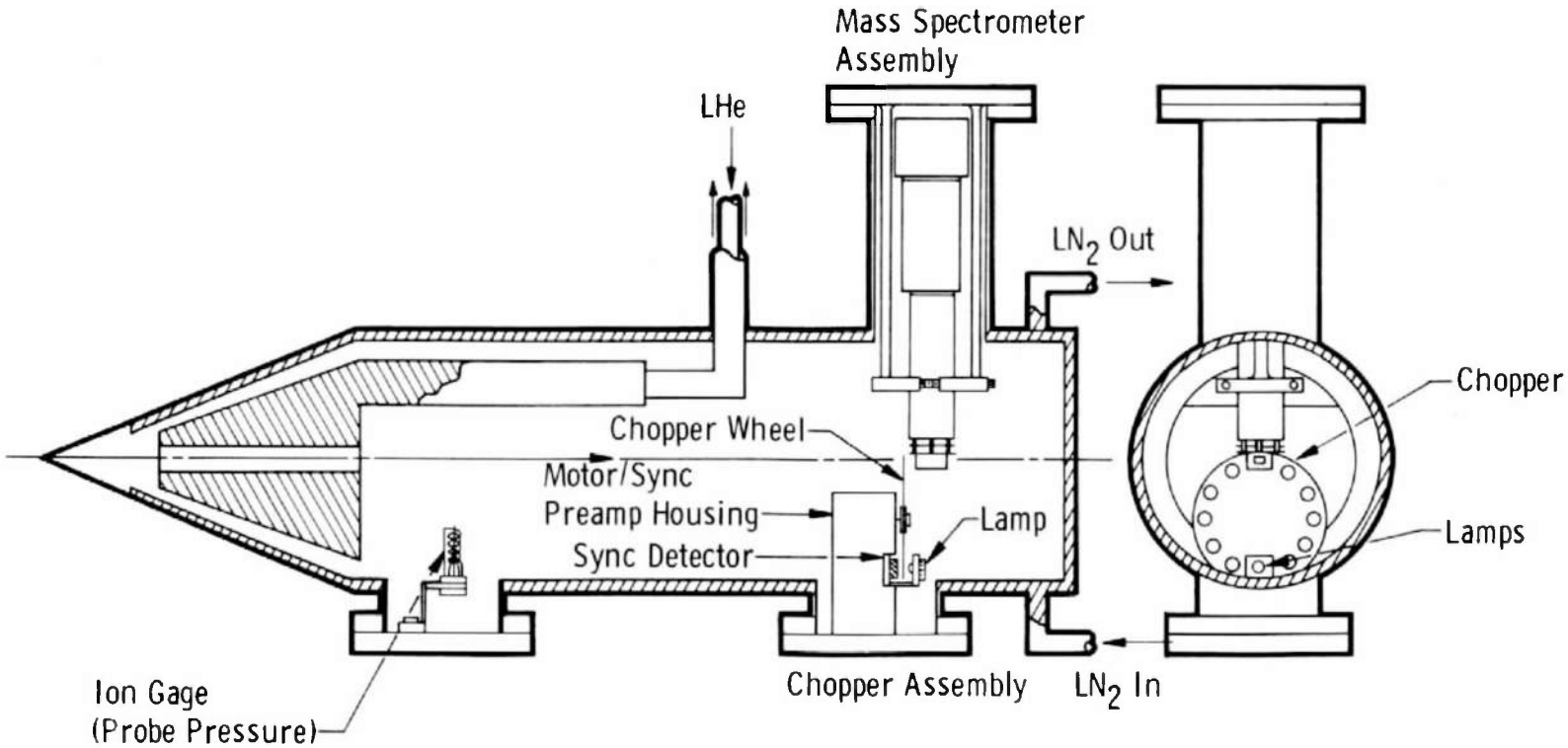

Fig. 2 Schematic of Probe Assembly in the Configuration for Species Identification and Density Measurements

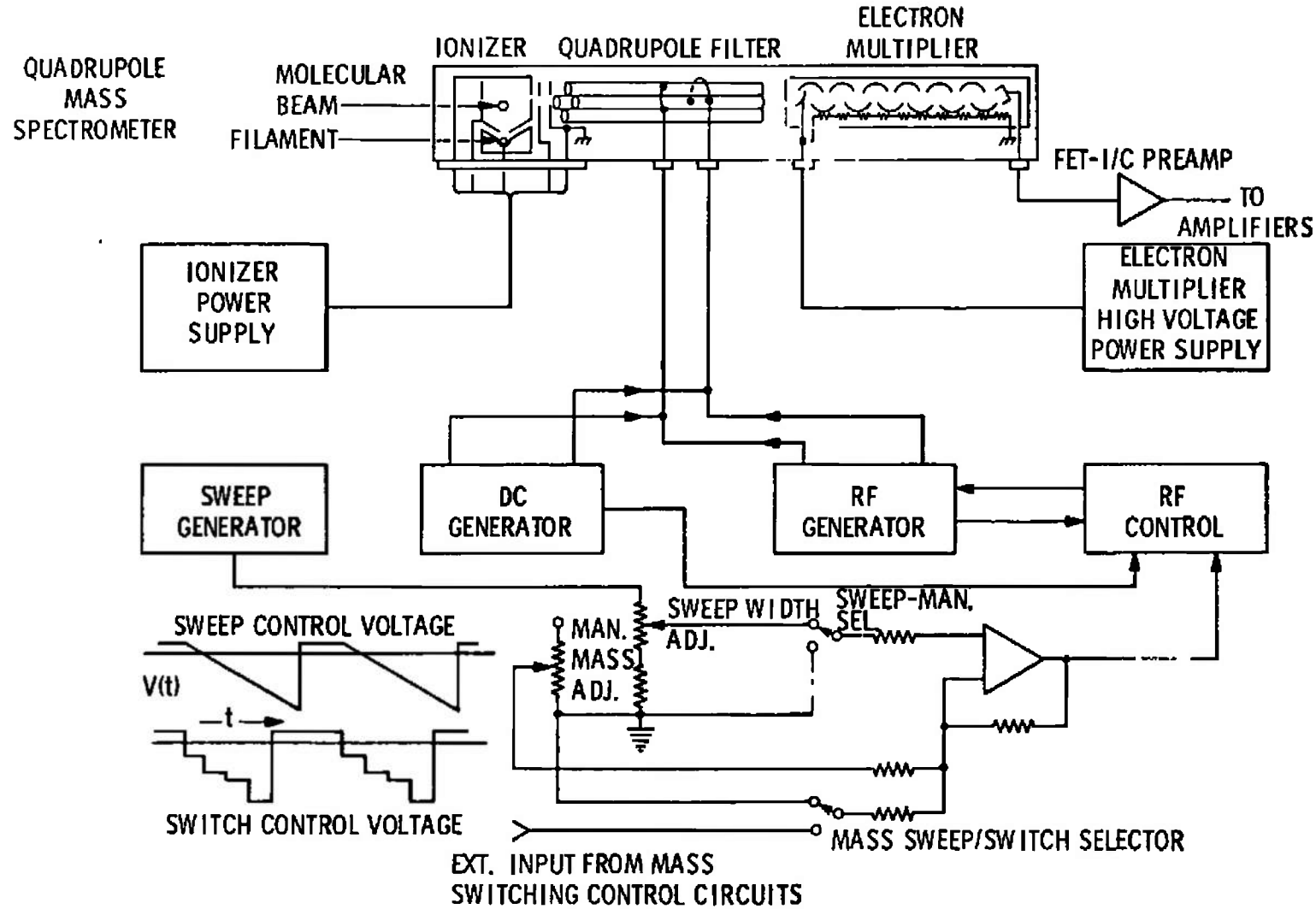

Fig. 3 Block Diagram of Typical Quadrupole Mass Spectrometer with Mass Switching Input Control

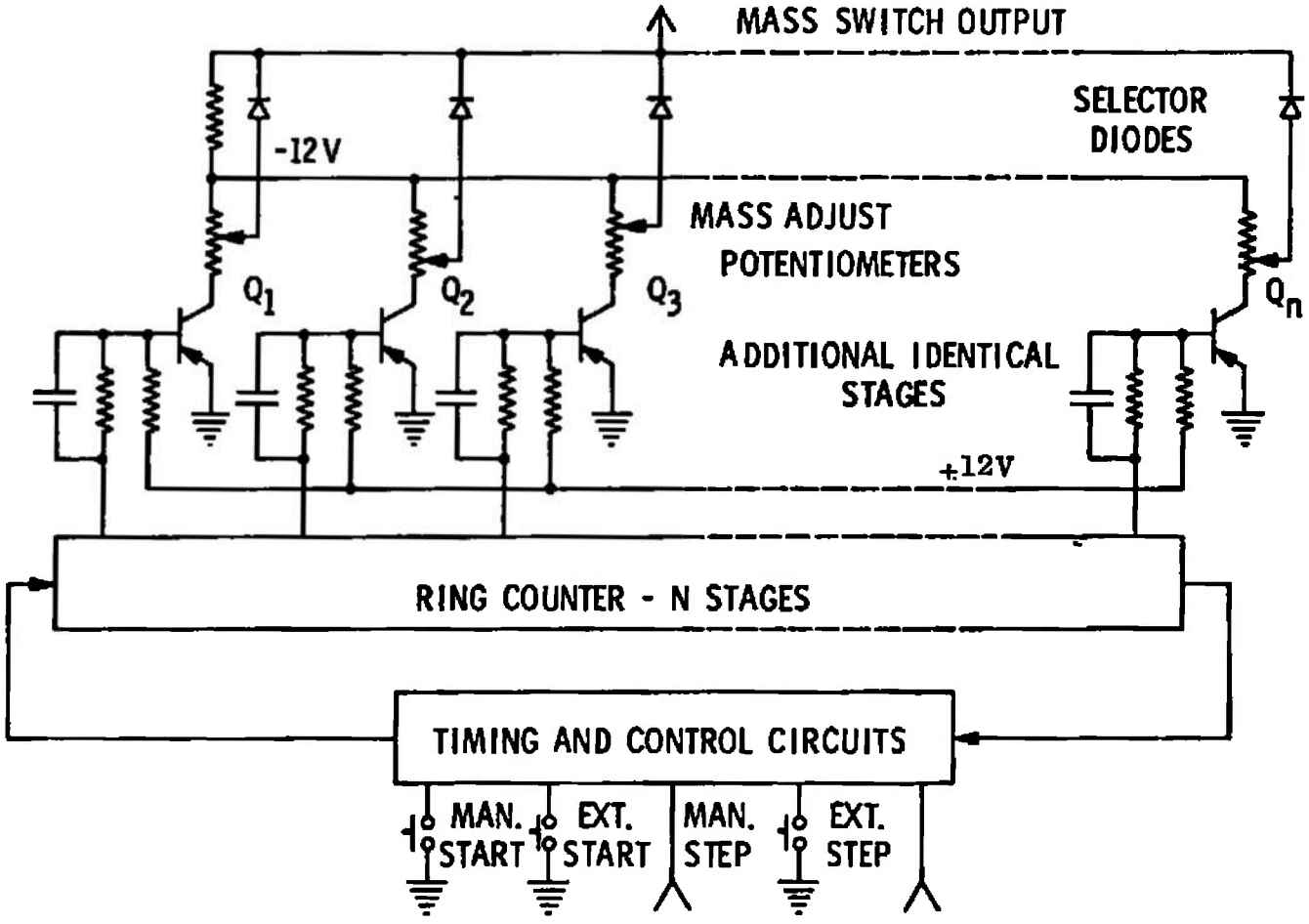

Fig. 4 Block Diagram of Mass Switching Control Unit for Quadrupole Mass Spectrometer

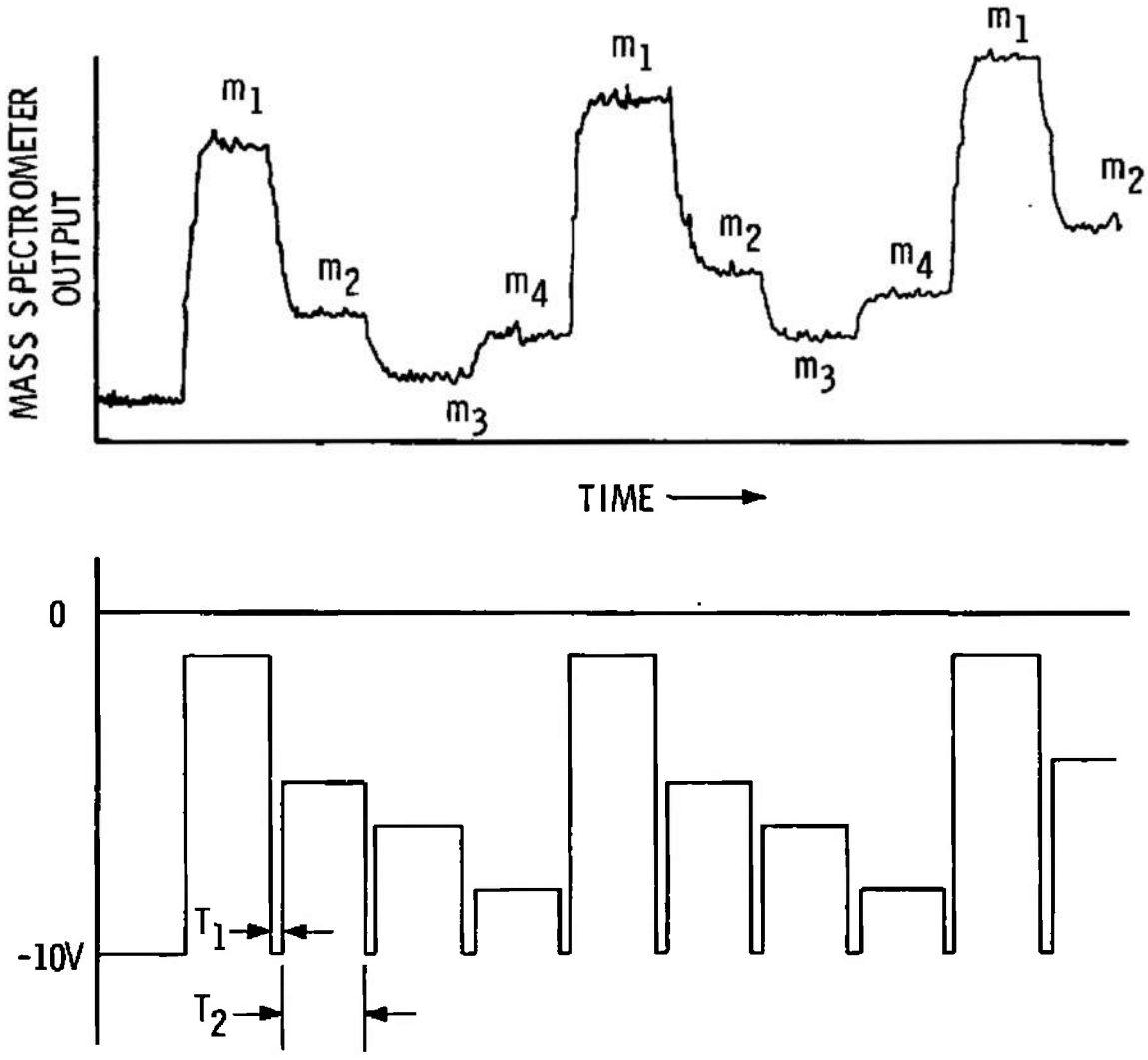

Fig. 5 Mass Spectrometer Waveforms Using Rapid Mass Switching Control Unit

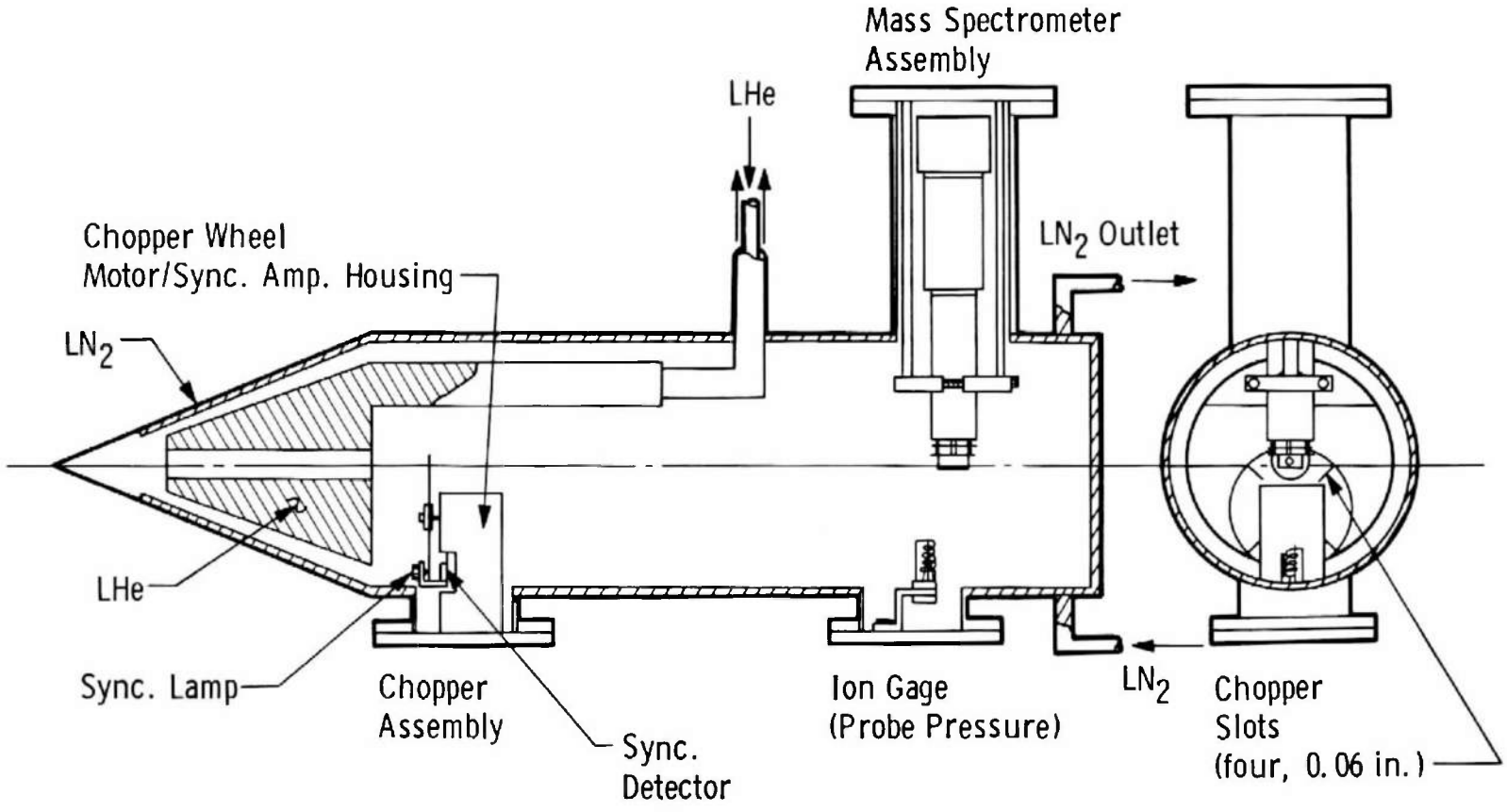

Fig. 6 Schematic of Probe Assembly in the Configuration for the Measurement of Velocity Distributions

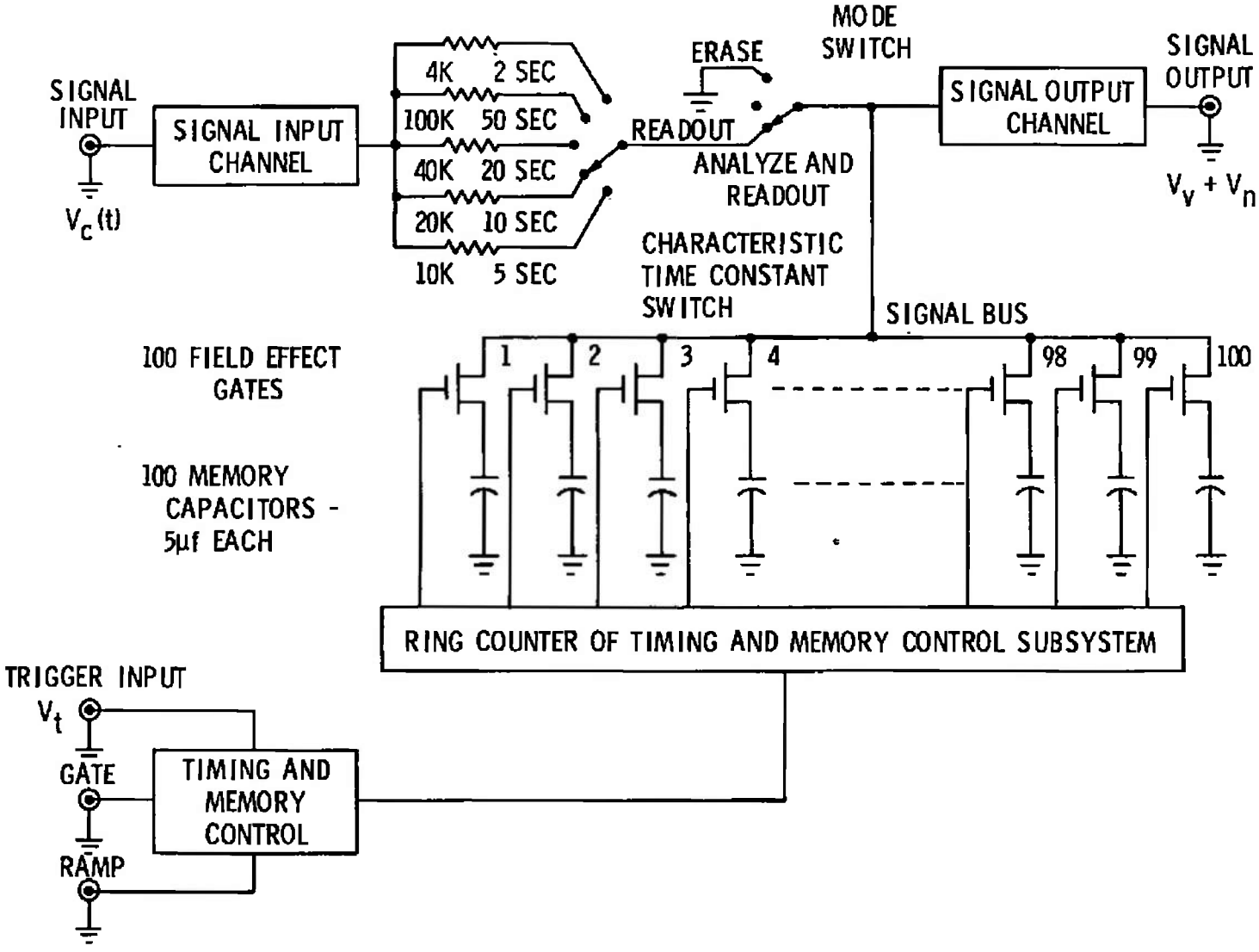

Fig. 7 Block Diagram of Waveform Eductor

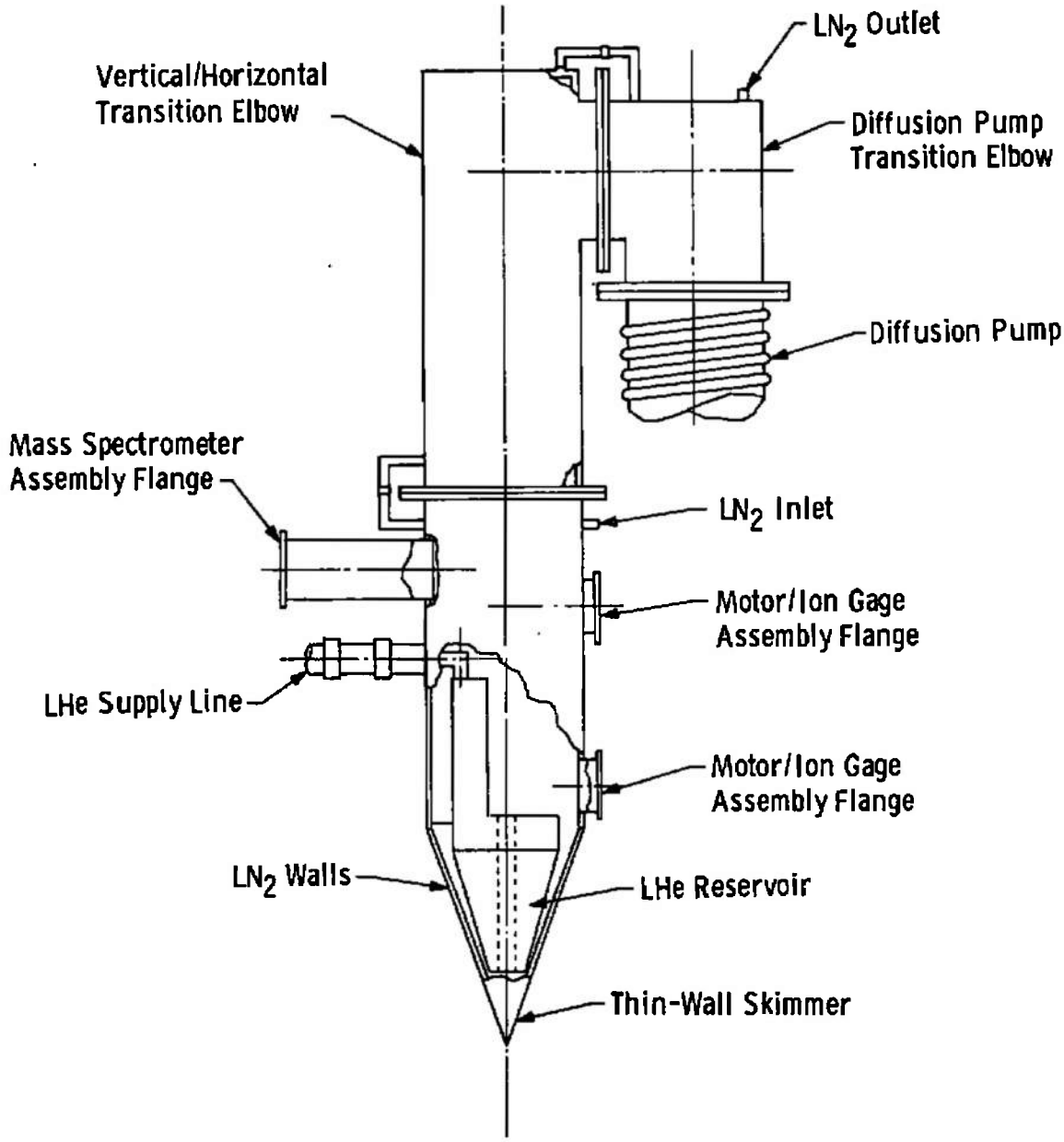

Fig. 8 Mechanical Features of Spectrometer Probe Shown for Vertical Mounting

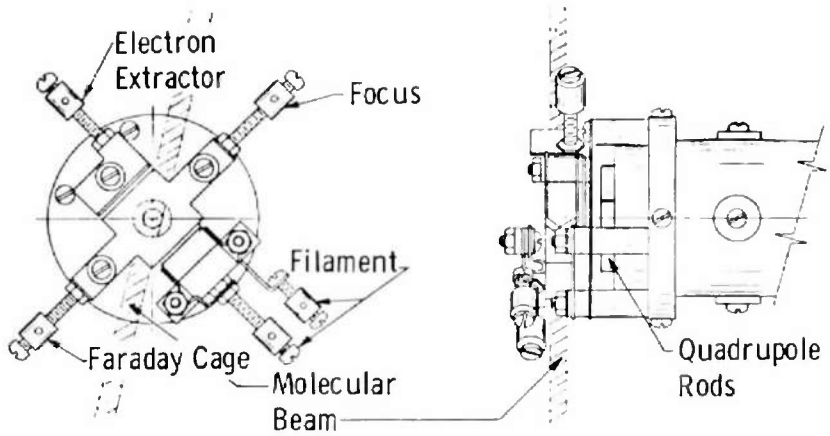

Fig. 9 Mass Spectrometer Ion Source

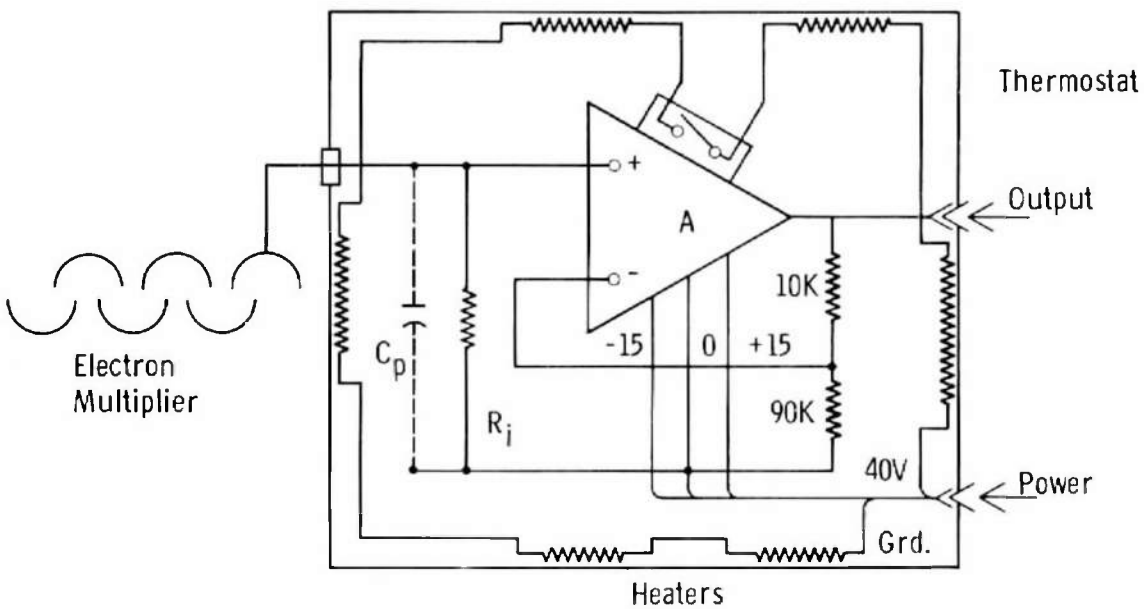

C_p - 3-pfd Shunting Capacitance

R_i - 0.5/1-megawatt Input Resistor

A - High Gain, Fast Rise Time, FET Input Operational Amplifier

Fig. 10 Mass Spectrometer Input Preamplifier

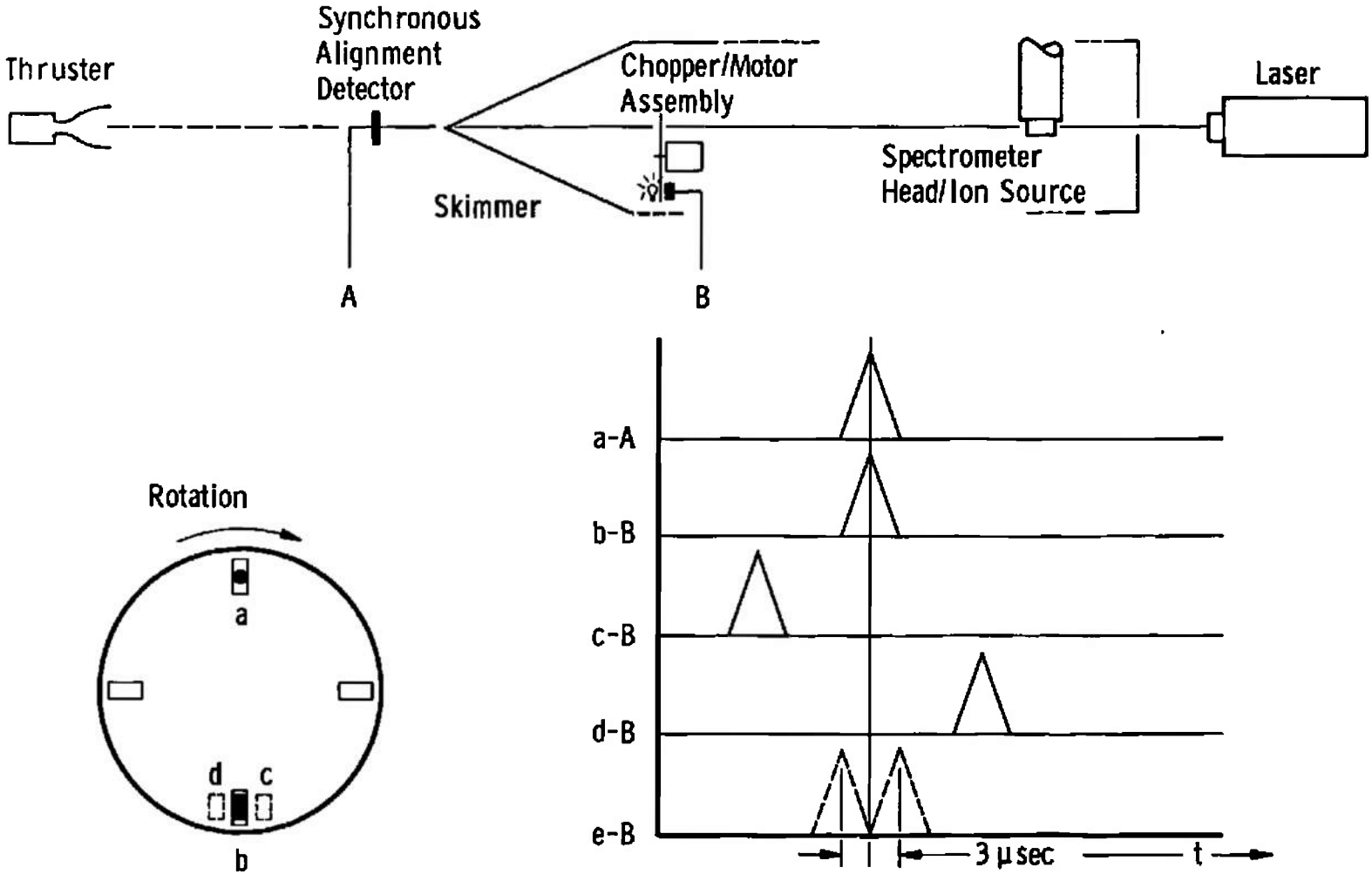

Fig. 11 Synchronous Pulse Alignment Conditions

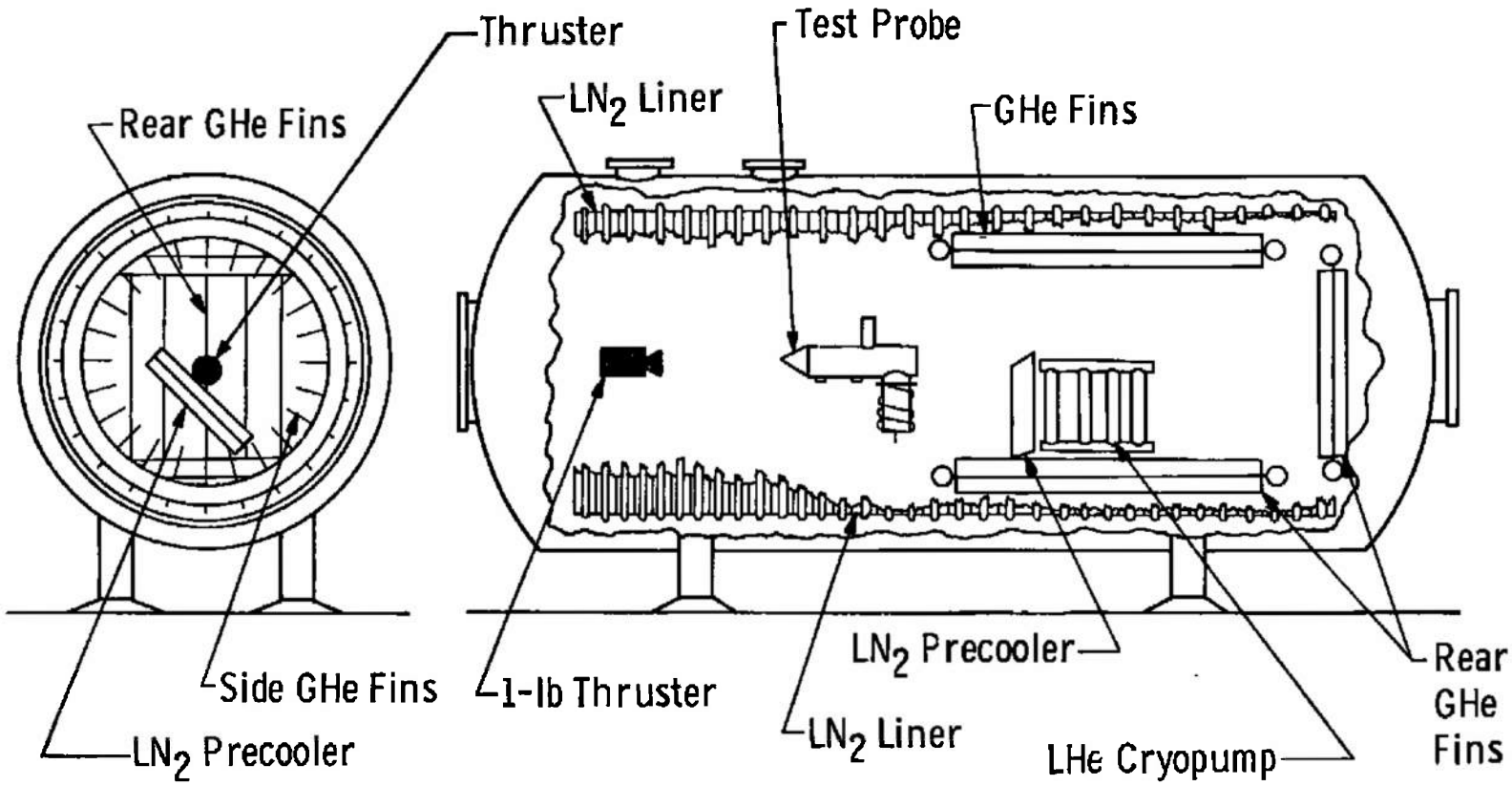

Fig. 12 Aerospace Research Chamber (10V)

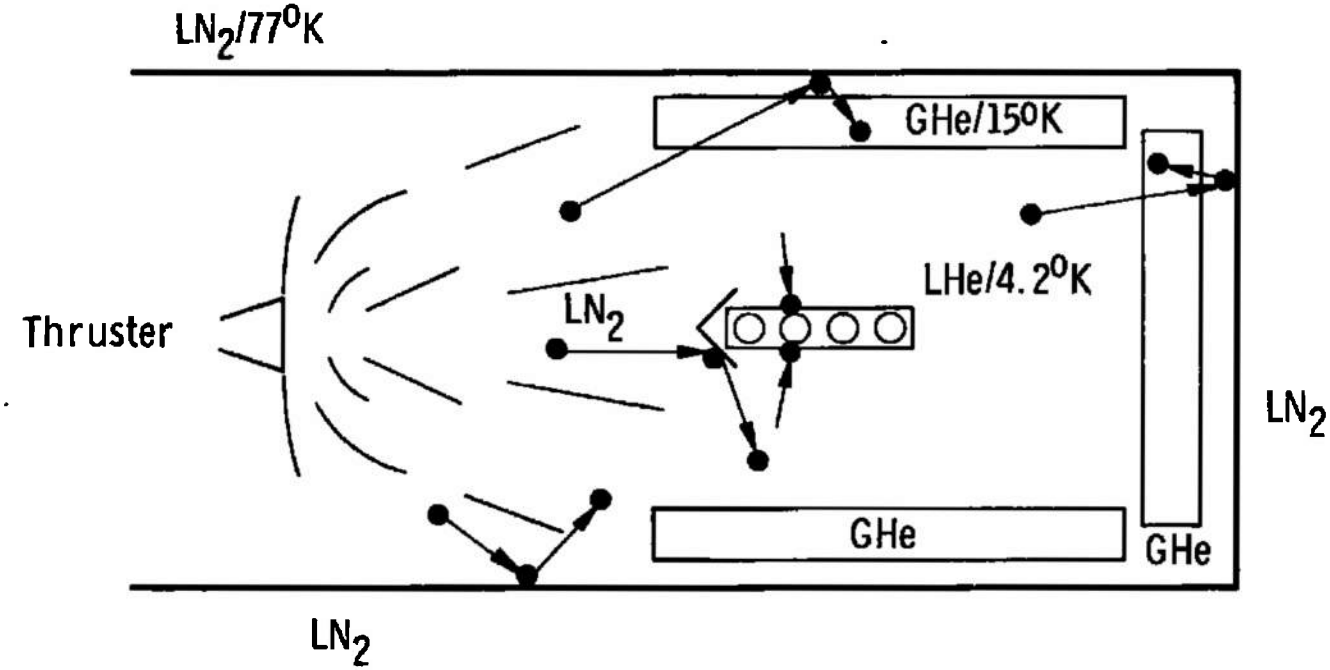

Fig. 13 Cryogenic Pumping Configuration of Chamber 10V

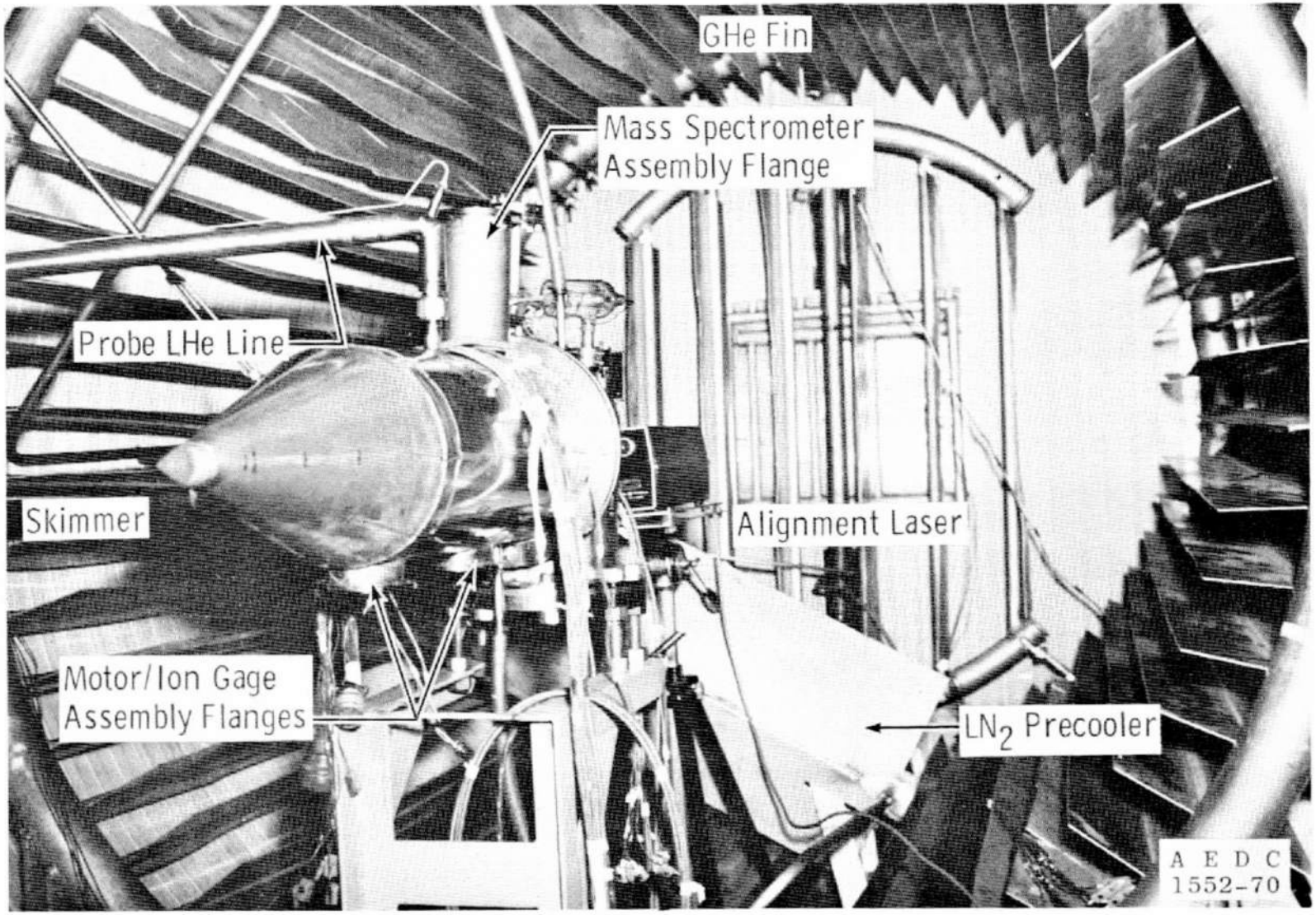

Fig. 14 Mass Spectrometer Probe Installation in Chamber 10V

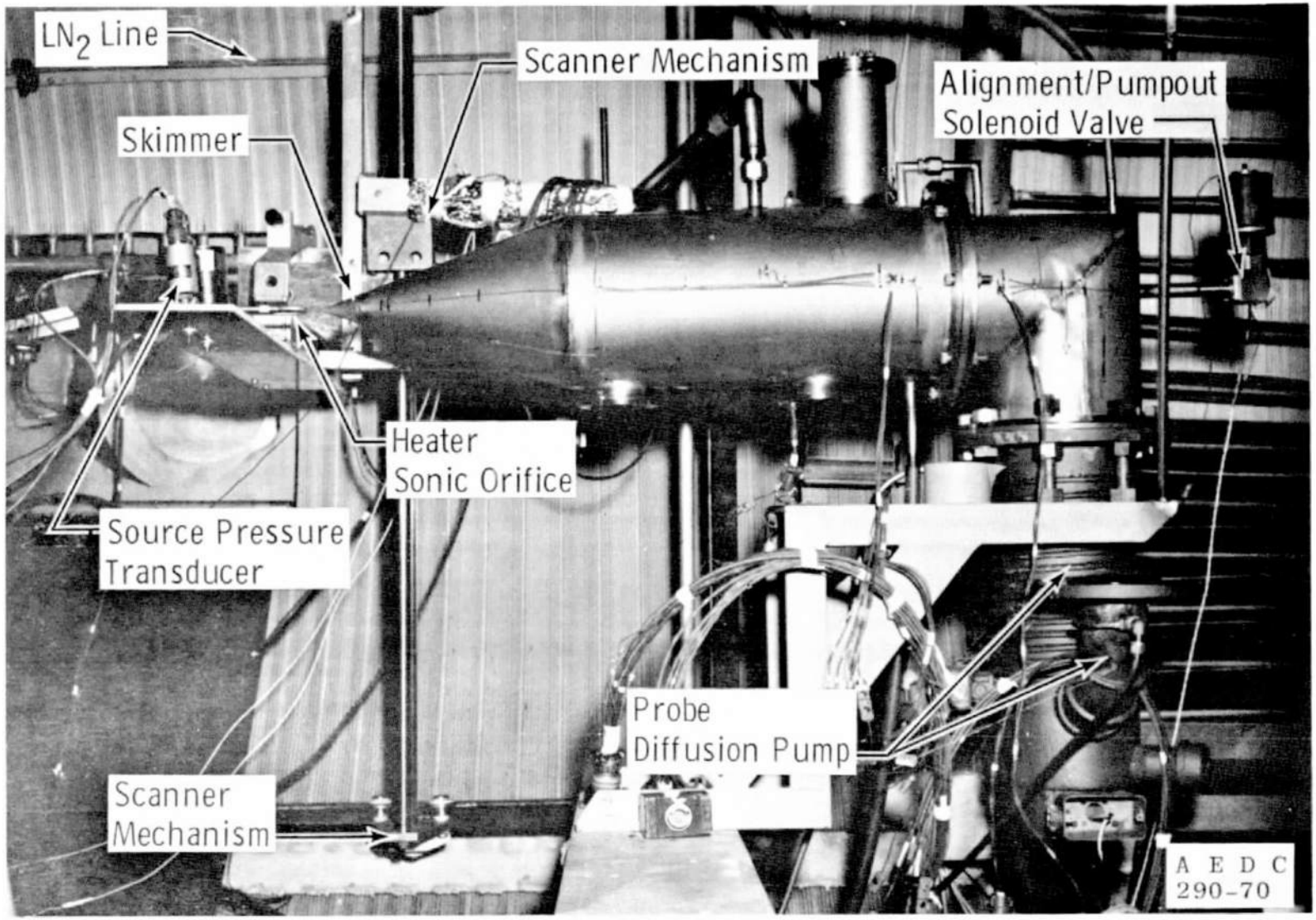

Fig. 15 Chamber Installation for Sonic Orifice as a Gas Source

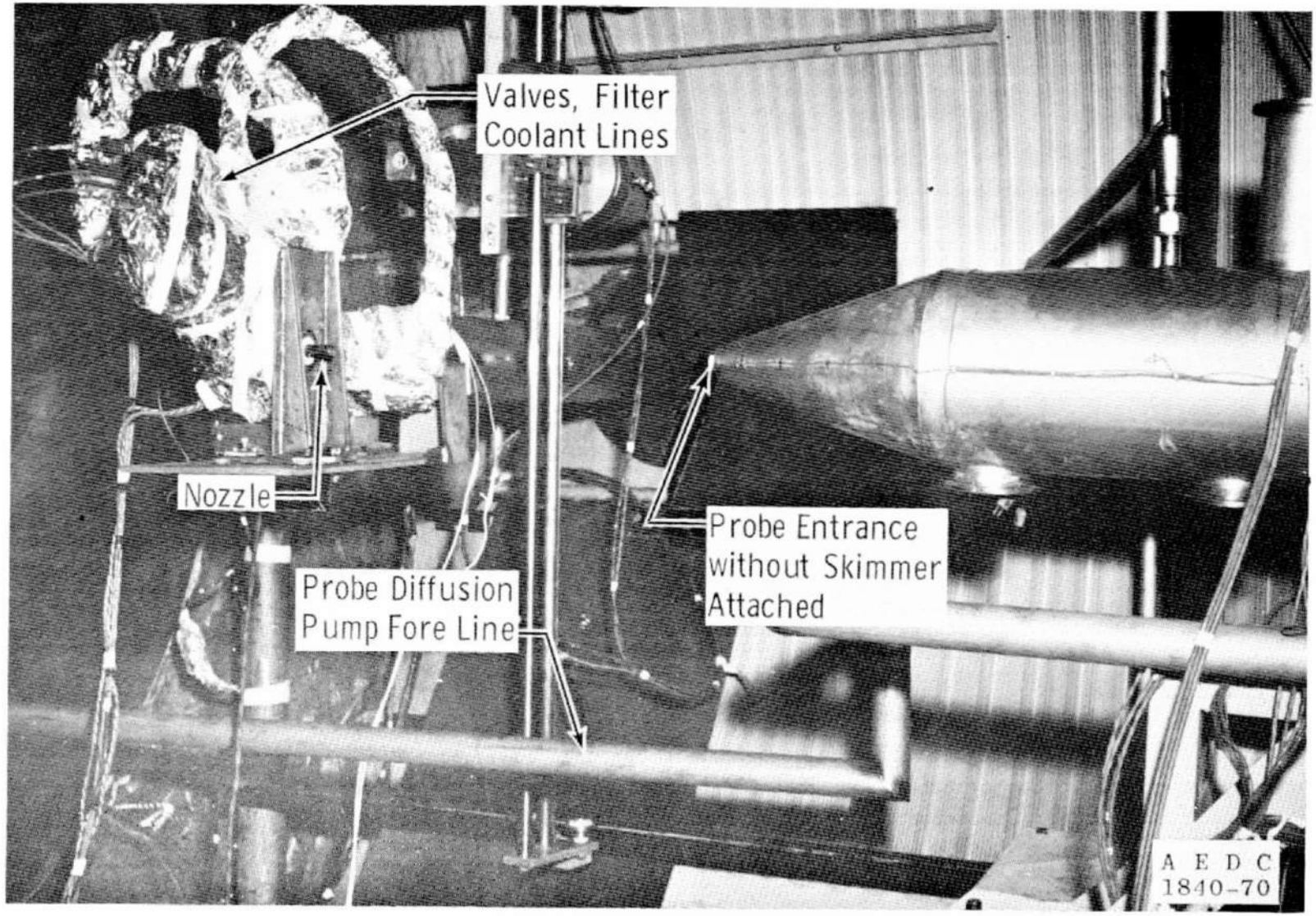

Fig. 16 Chamber Installation for Rocket as Gas Source

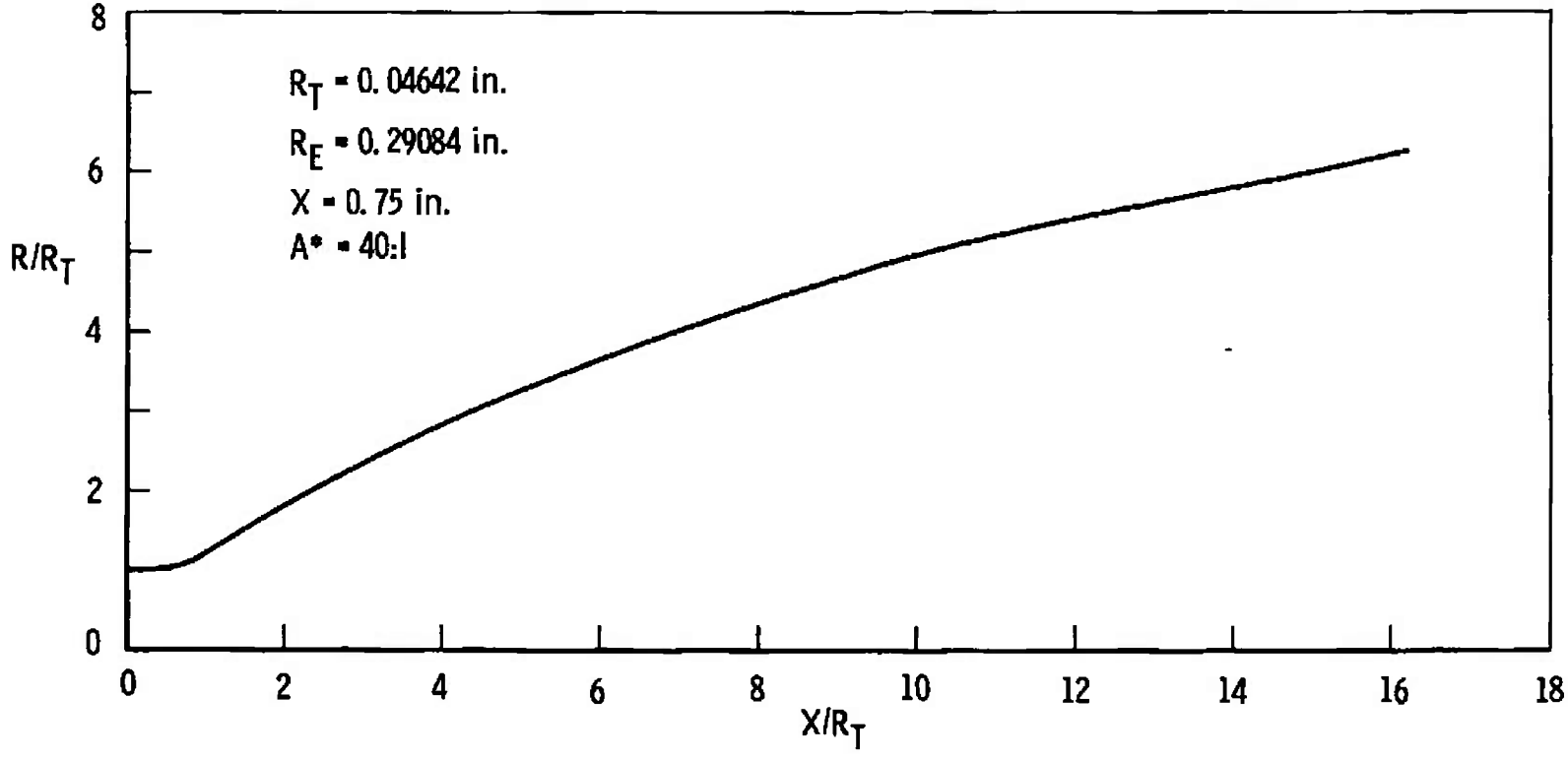

Fig. 17 Nozzle Contour of MOL-Scaled Thruster

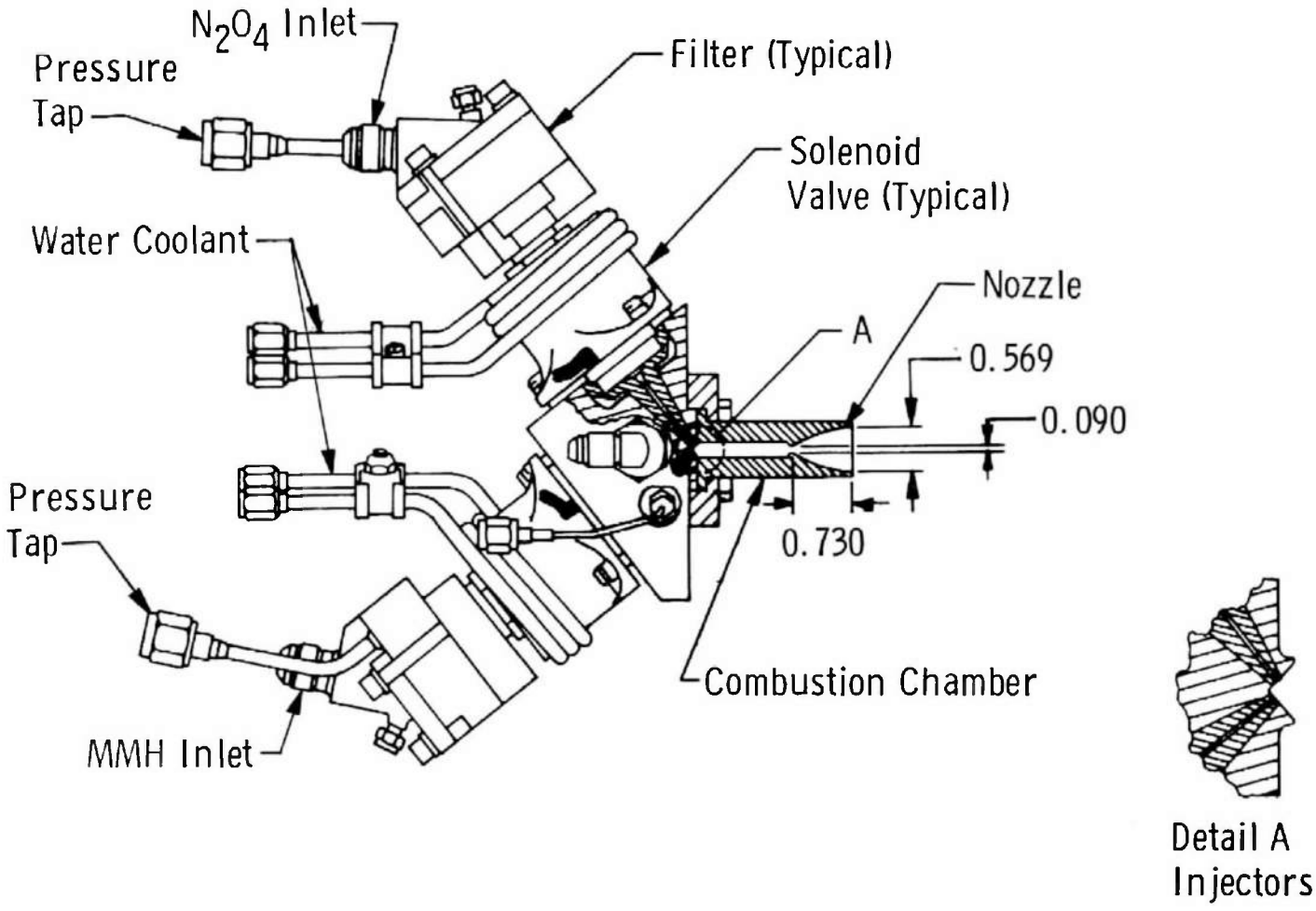

Fig. 18 One-Pound-Thrust Engine and Valves

Filter Time Constant - 10 msec
Chopper Rotation Speed - 250 rev/sec
Oscilloscope Sweep Speed - 0.2 sec/div
Mass Spectrometer Switch Rate - 100 msec/step

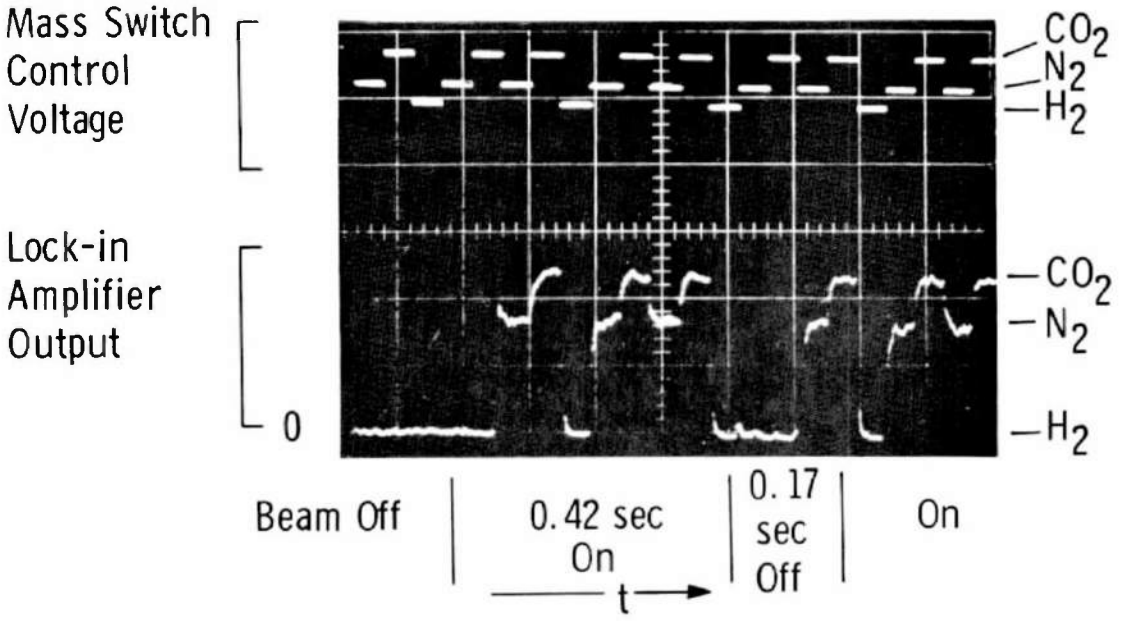

a. Roll-Off 6 db/Octave

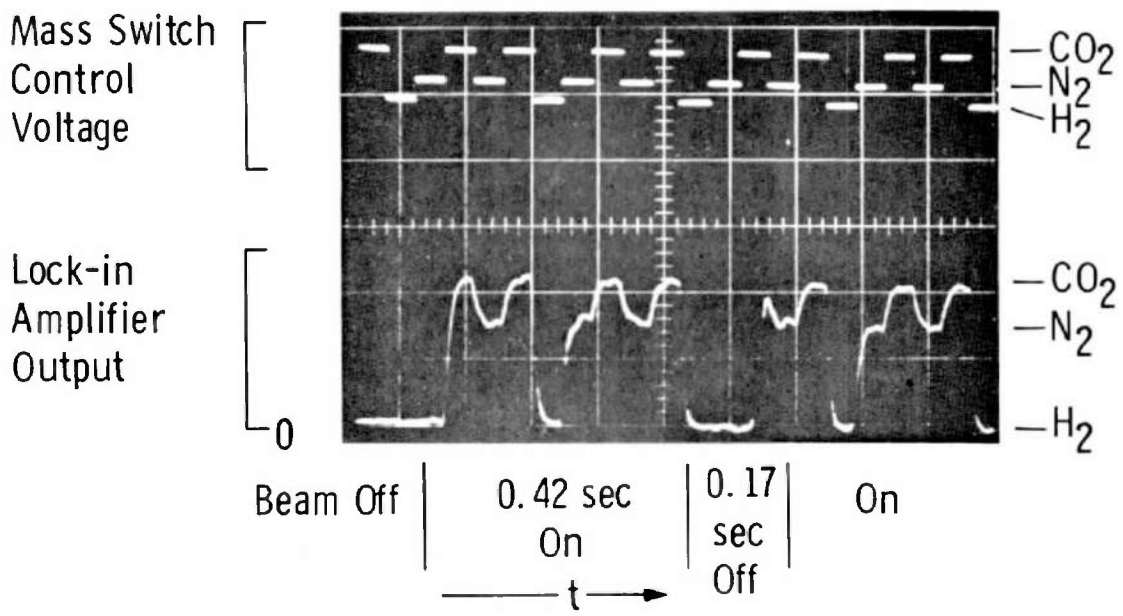

b. Roll-Off 12 db/Octave

Fig. 19 Oscilloscope Traces of Sampling Process Using Lock-In Amplifier and Mass Switching Technique

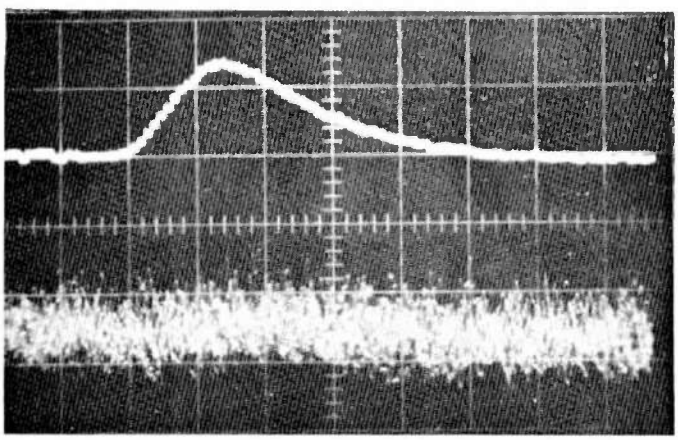

Fig. 20 Eductor Input-Output Waveforms for a Typical Distribution Function

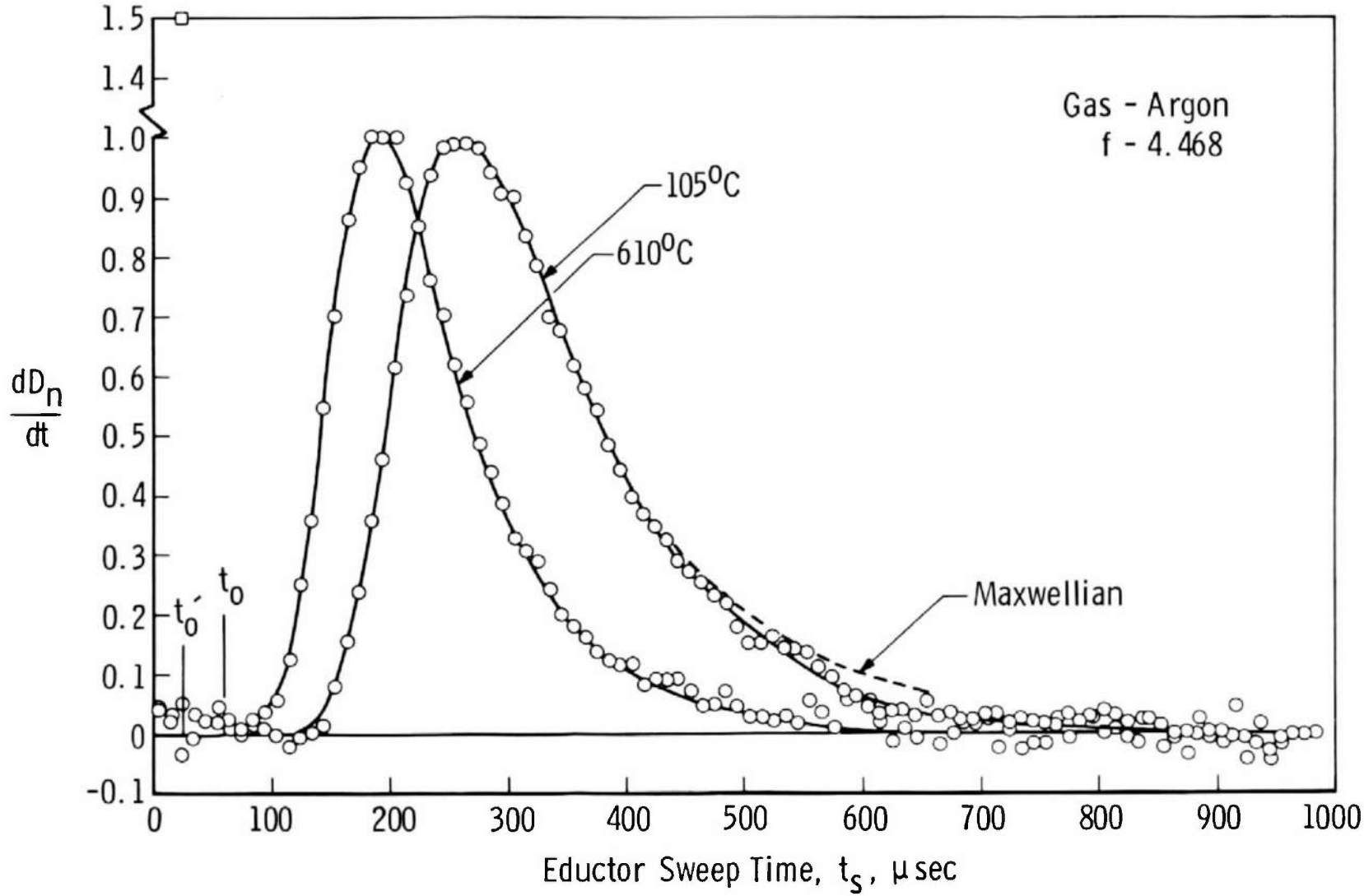

Fig. 21 Distributions for High Temperatures

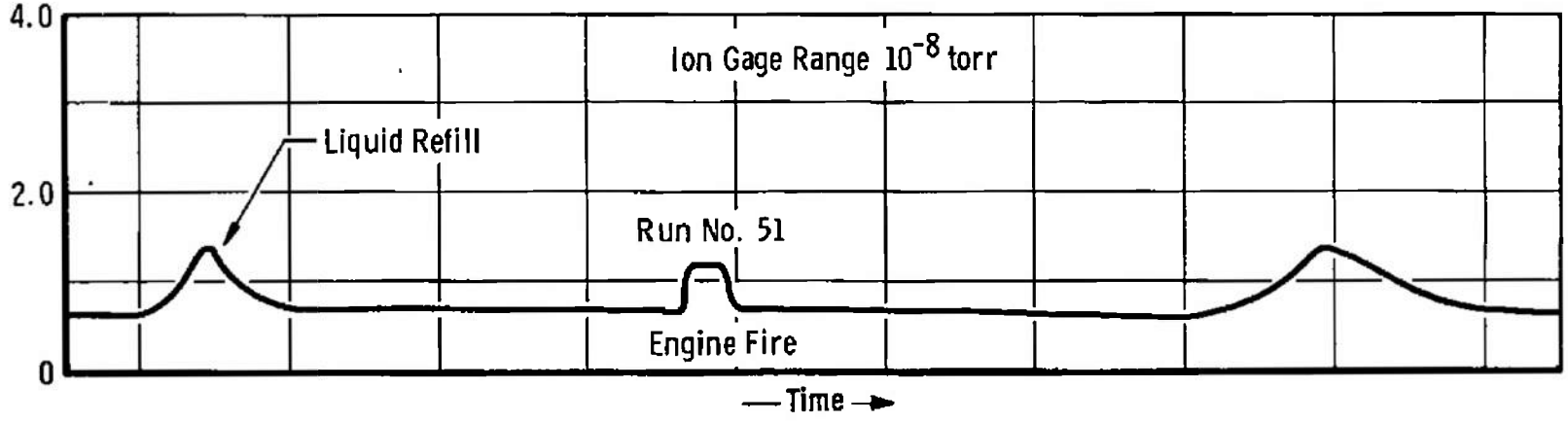

Fig. 22 Probe Pressure Response for 10-sec Rocket Firing

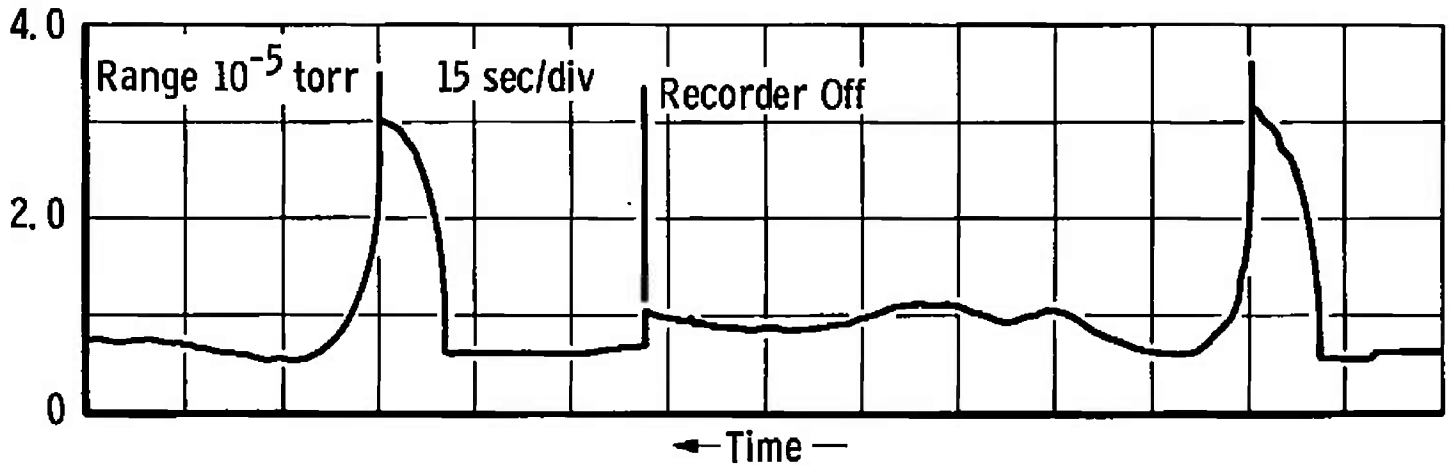

Fig. 23 Typical Chamber 10V Background Pressure Response for Two 10-sec Thruster Firings

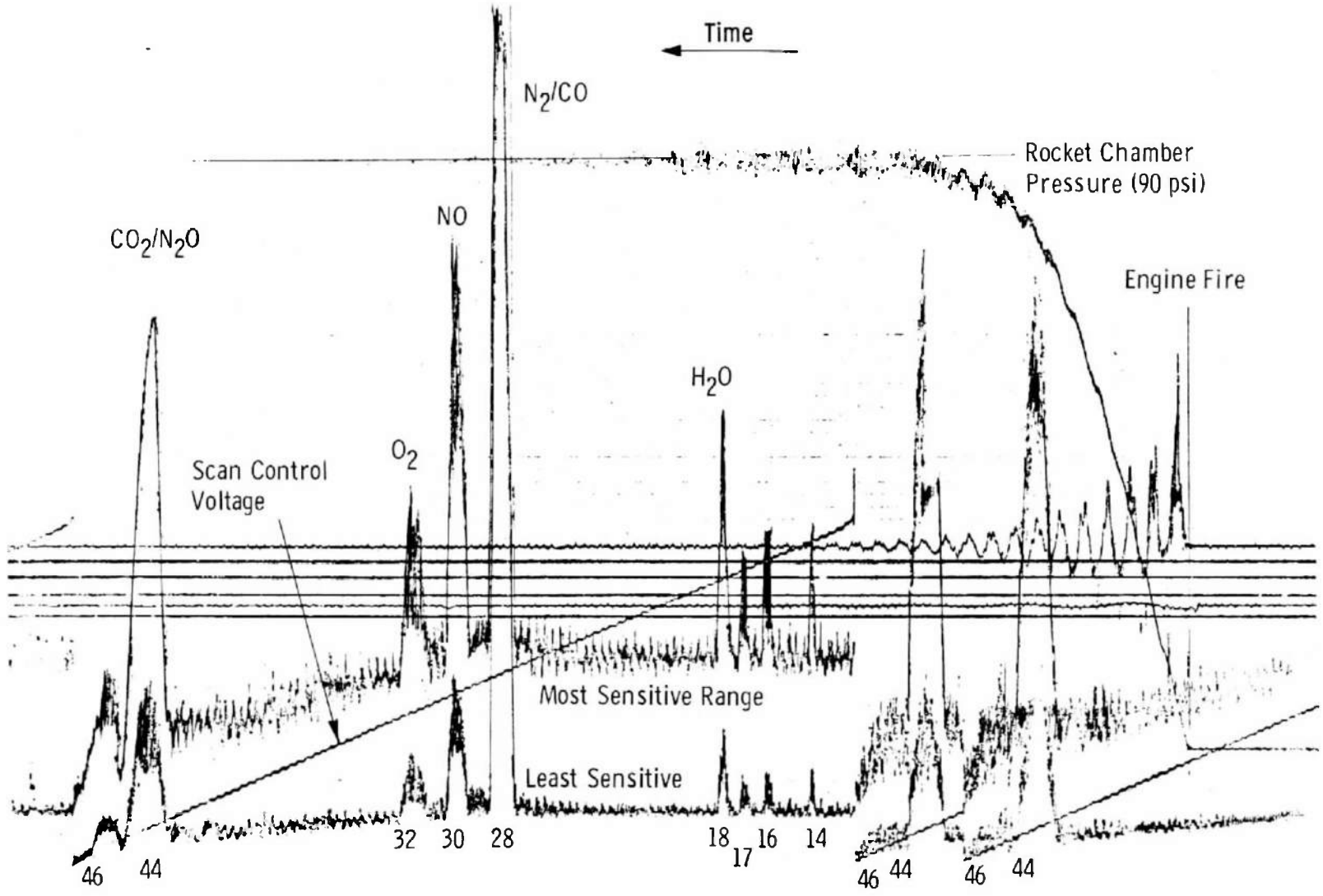

Fig. 24 Mass Spectrum of Rocket Exhaust for MMH/N_2O_4 and 1.6 O/F Ratio

AEDC-TR-71-135

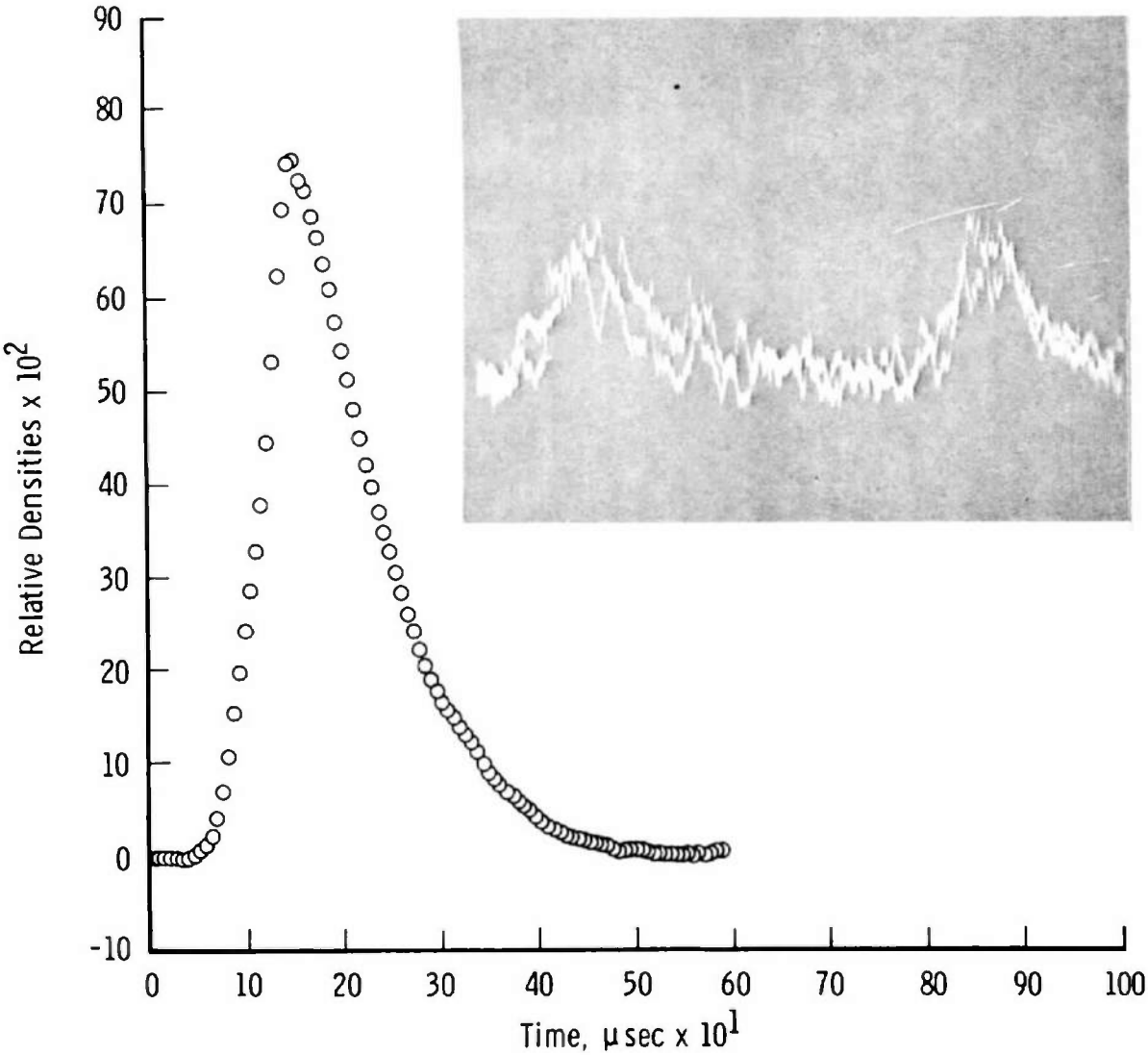

Fig. 25 Typical Time-of-Flight Distributions

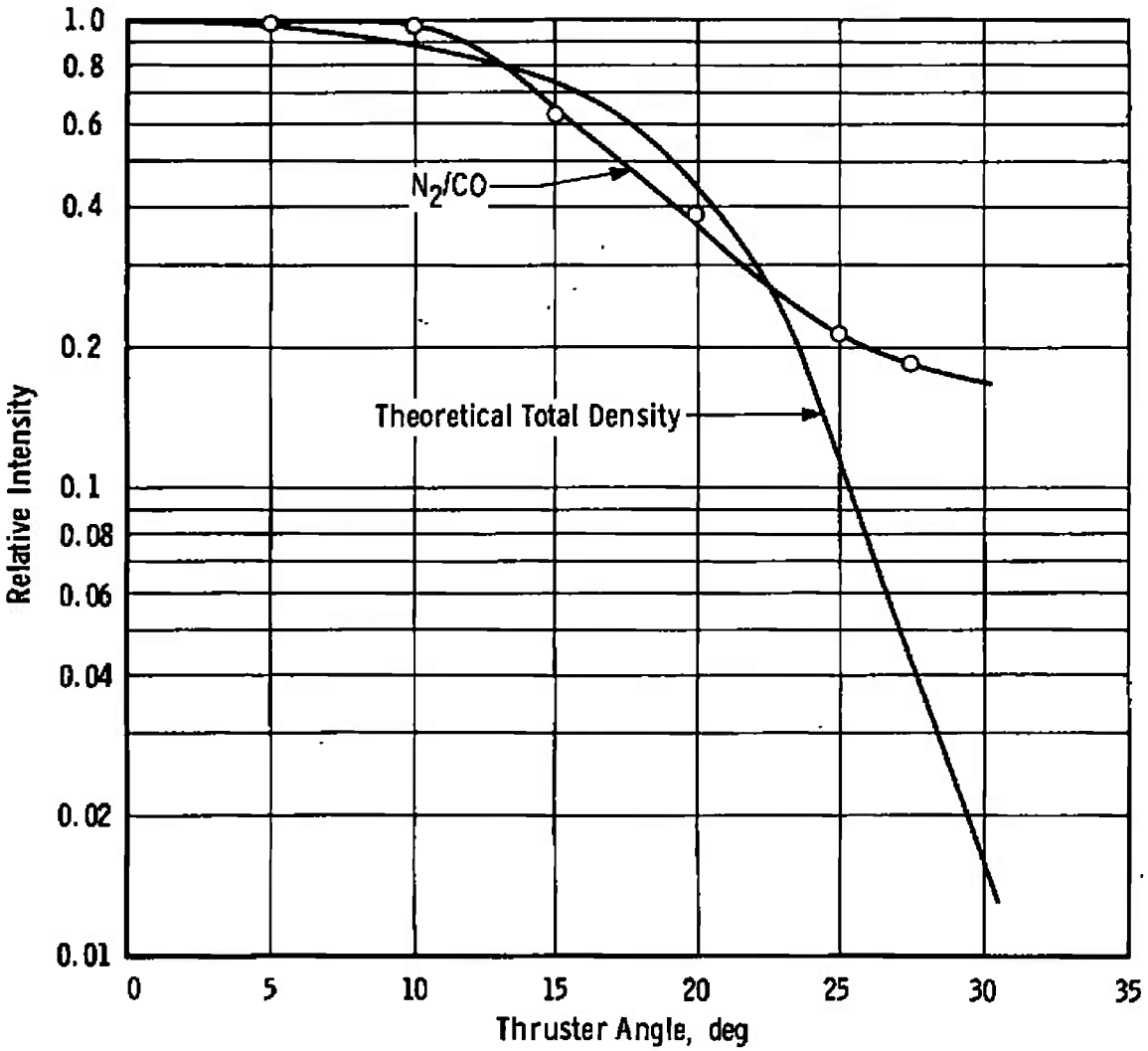

Fig. 26 Relative Intensity Variation with Engine Angle for Most Significant Specie, N_2/CO

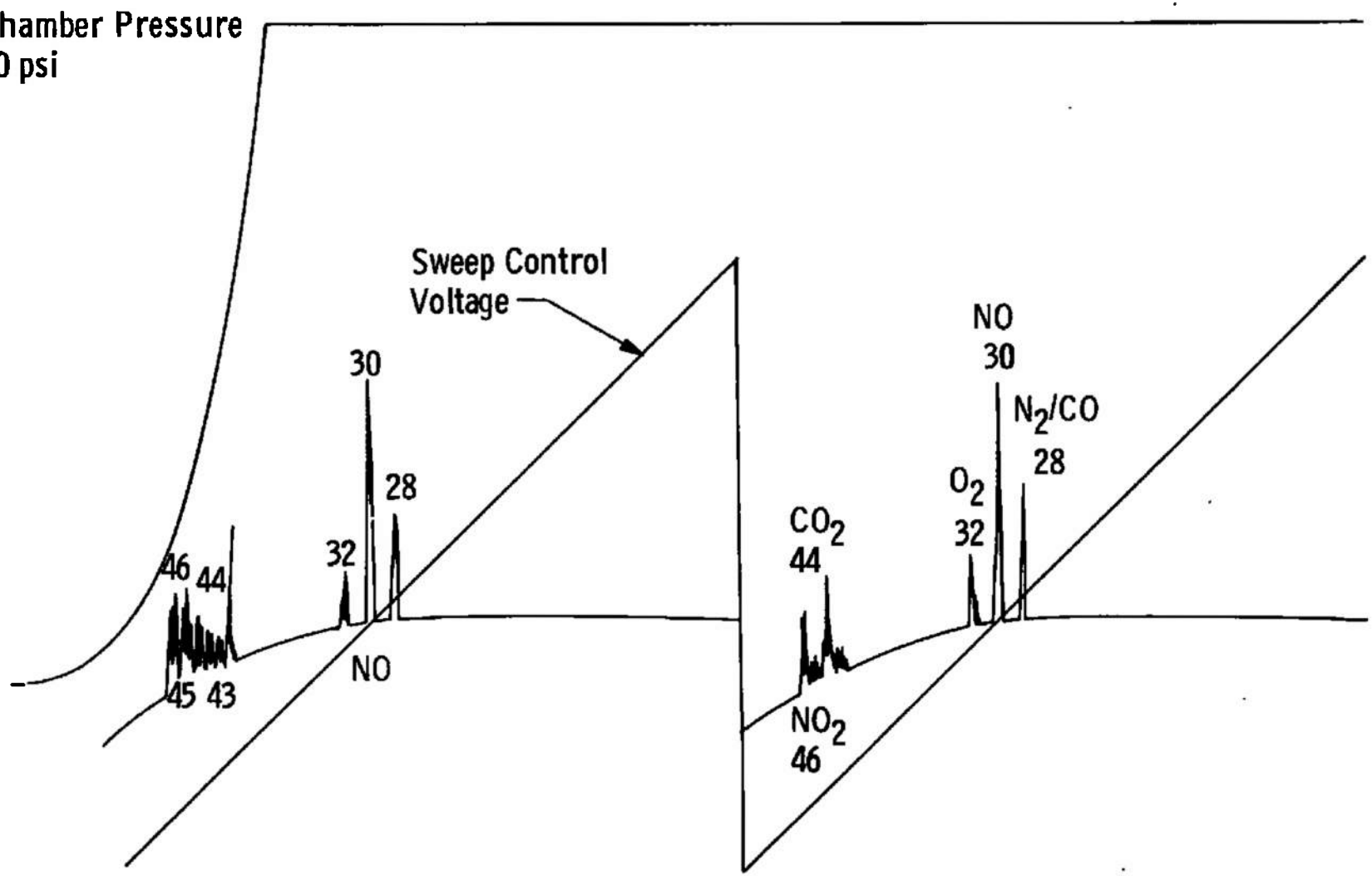

Fig. 27 Mass Spectrometer Scan for O/F Ratio of 1.9

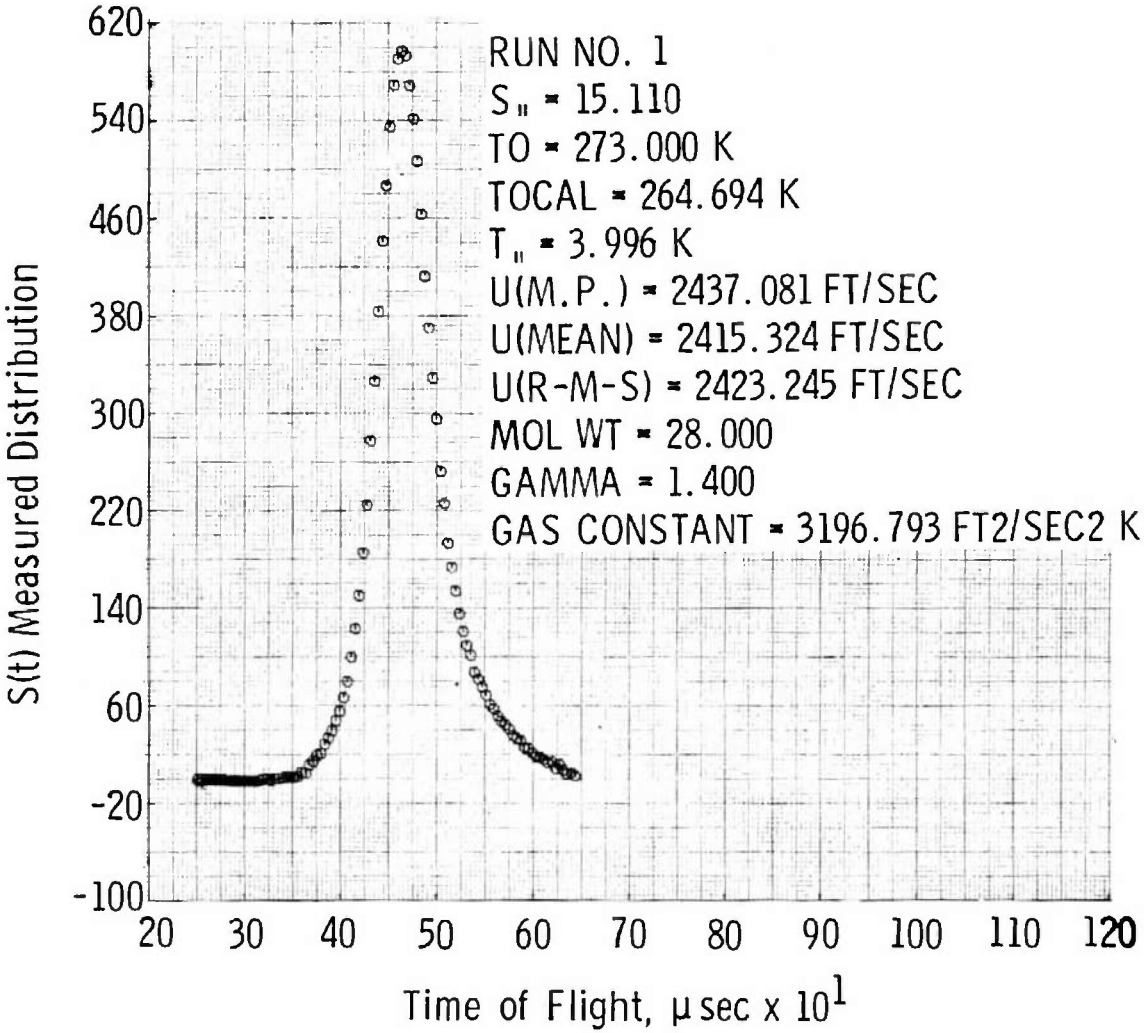

a. Time-of-Flight Distribution

Fig. 28 Nitrogen Time-of-Flight and Velocity Measurement for Expansion through Thruster Nozzle

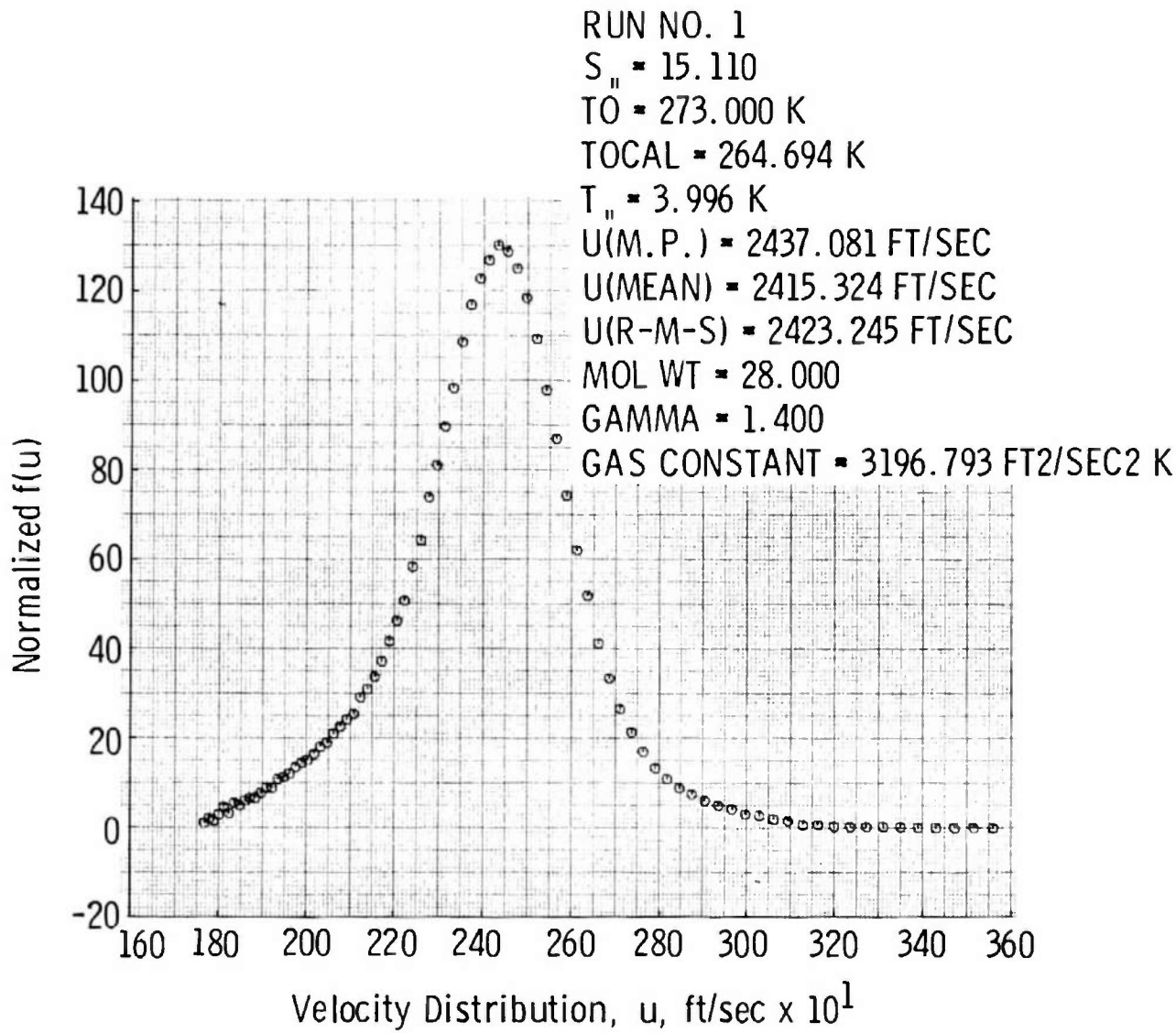

b. Velocity Distribution

Fig. 28 Concluded

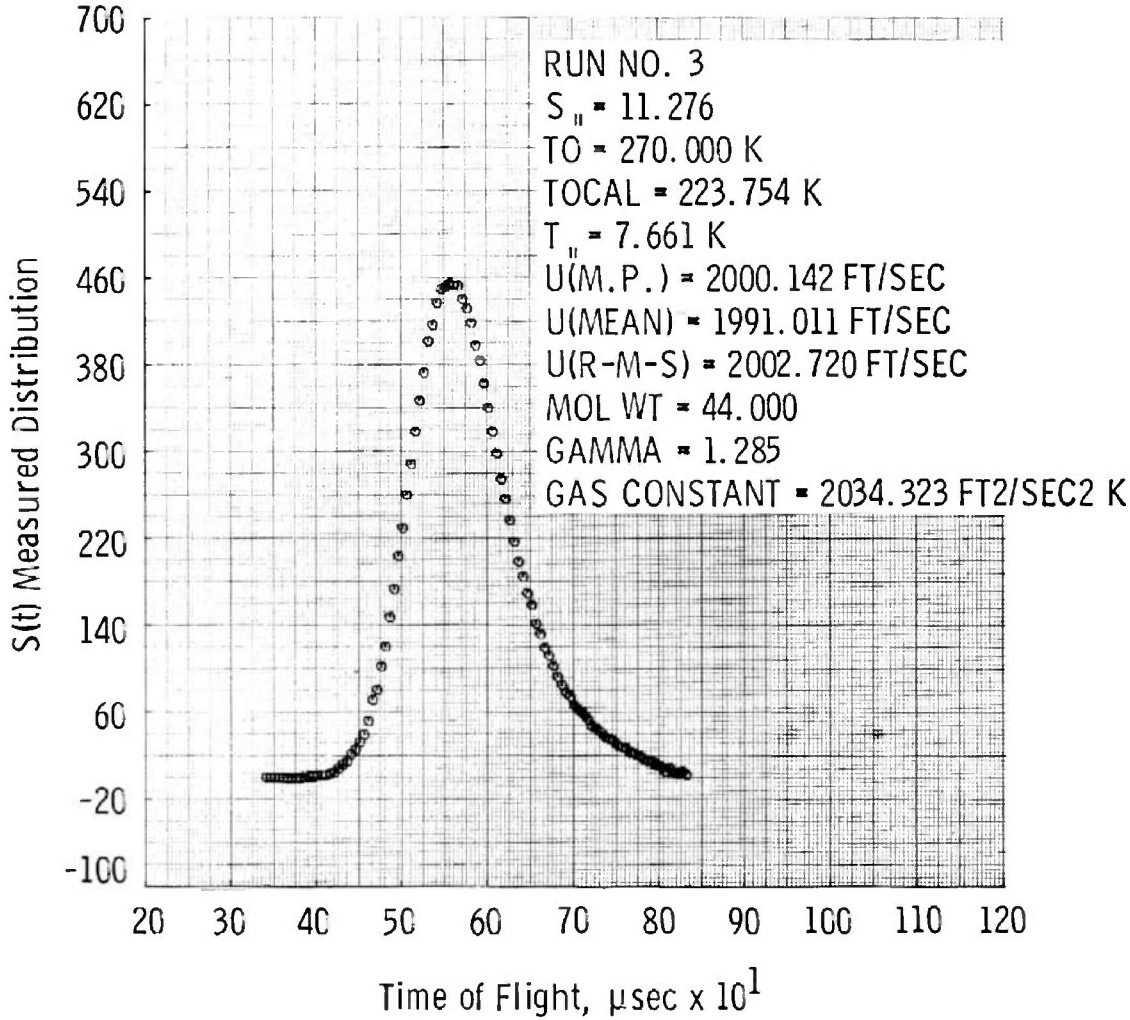

a. Time-of-Flight Distribution

Fig. 29 Carbon Dioxide Time-of-Flight and Velocity Measurement for Expansion through Thruster Nozzle

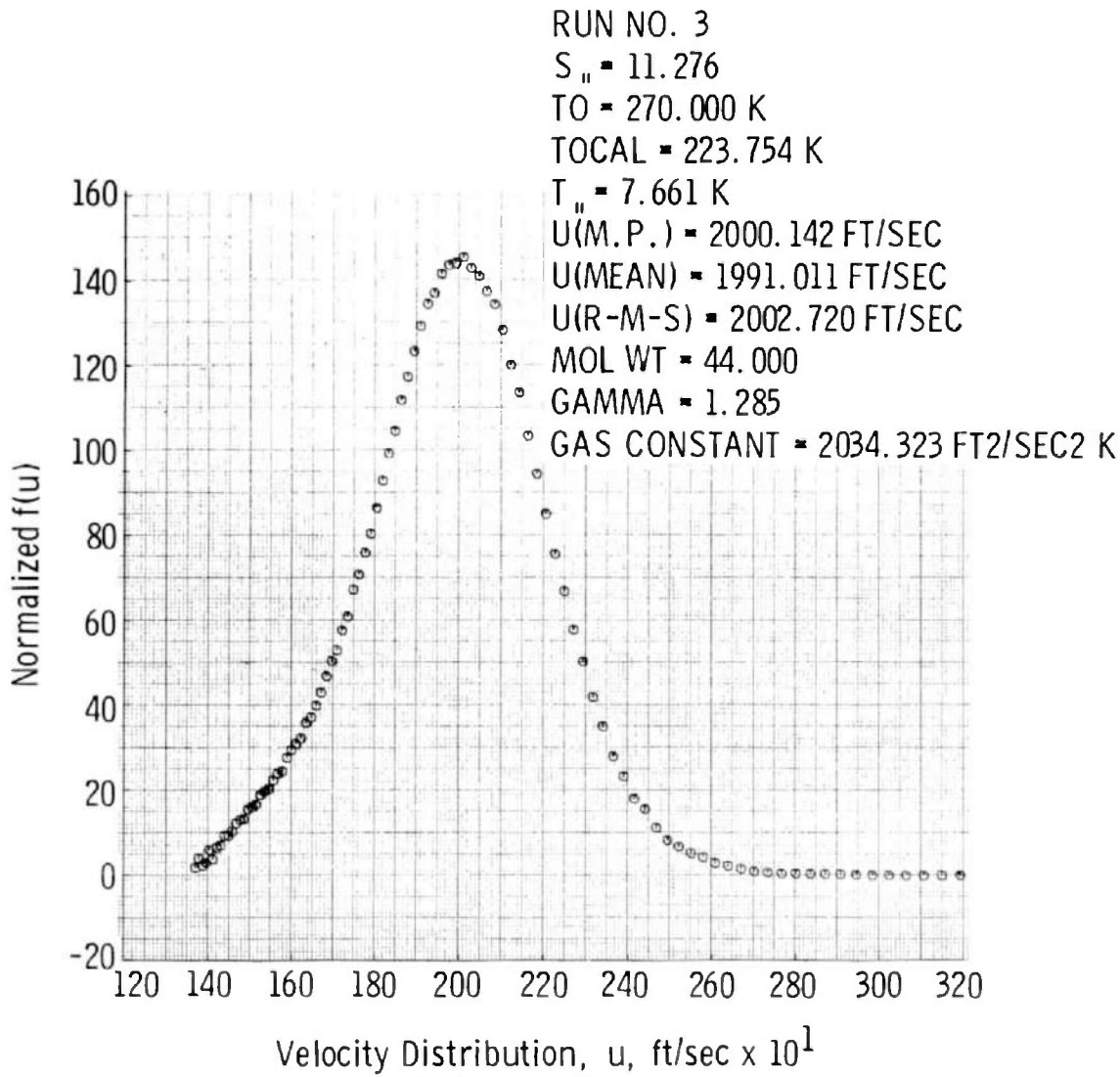

b. Velocity Distribution

Fig. 29 Concluded

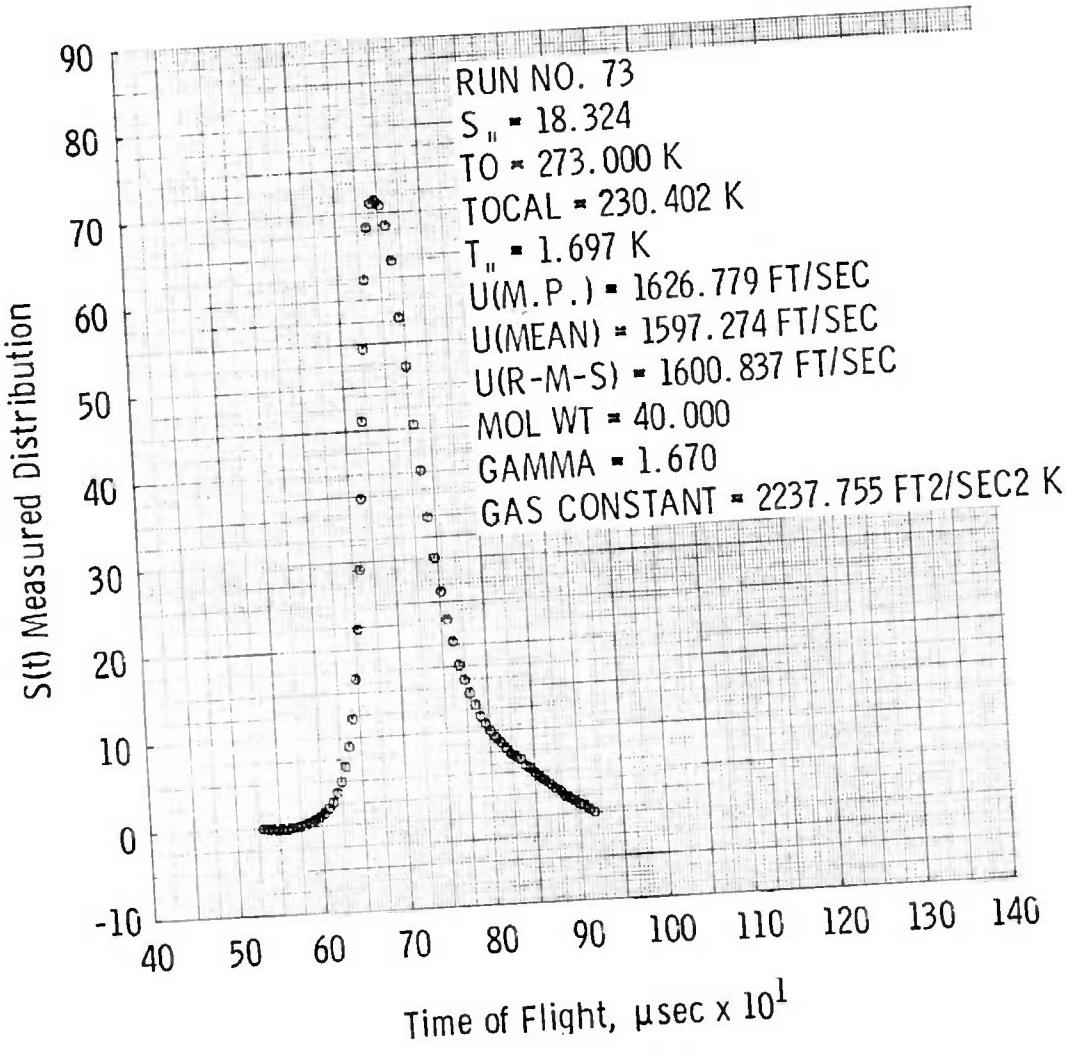

a. Time-of-Flight Distribution

Fig. 30 Argon Time-of-Flight and Velocity Measurement for Expansion from Sonic Orifice

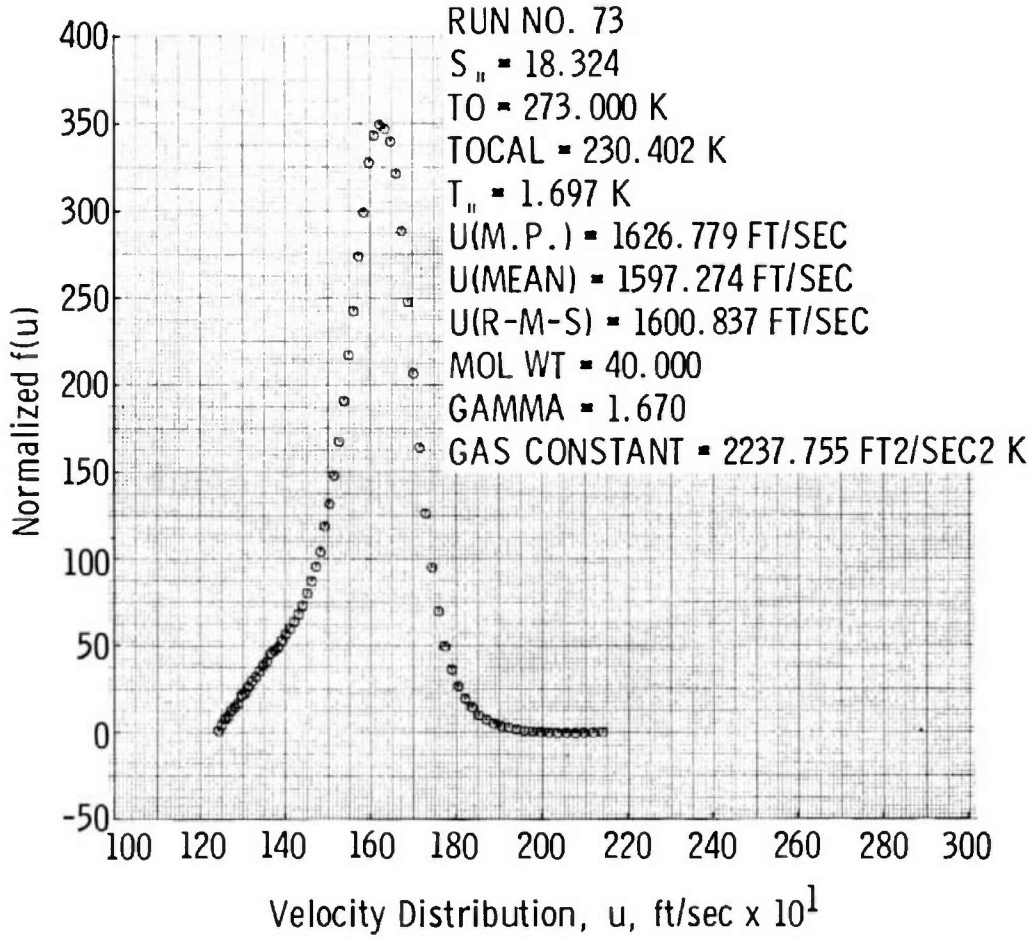

b. Velocity Distribution
Fig. 30 Concluded

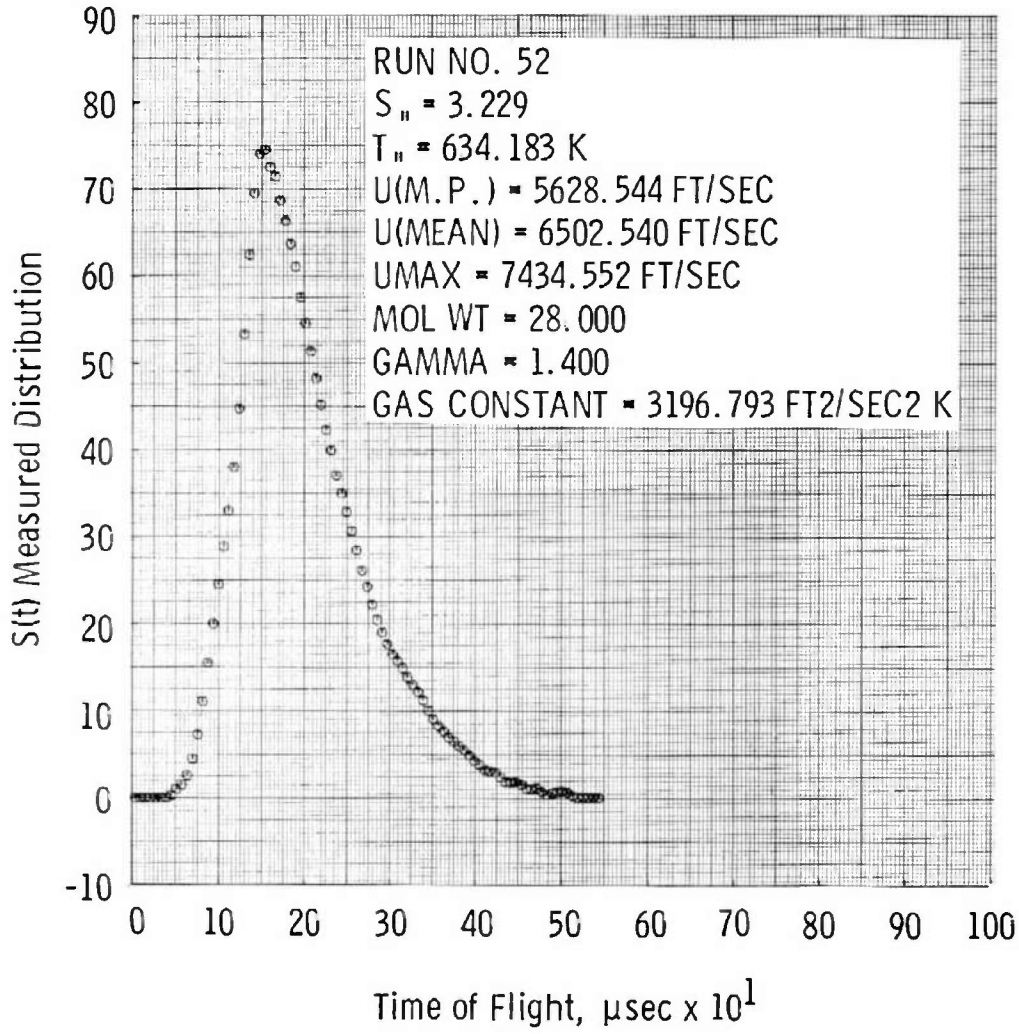

a. Time-of-Flight Distribution

Fig. 31 Nitrogen Time-of-Flight and Velocity Measurement for Hot Thruster Firing, U_{mp} = 5629 ft/sec

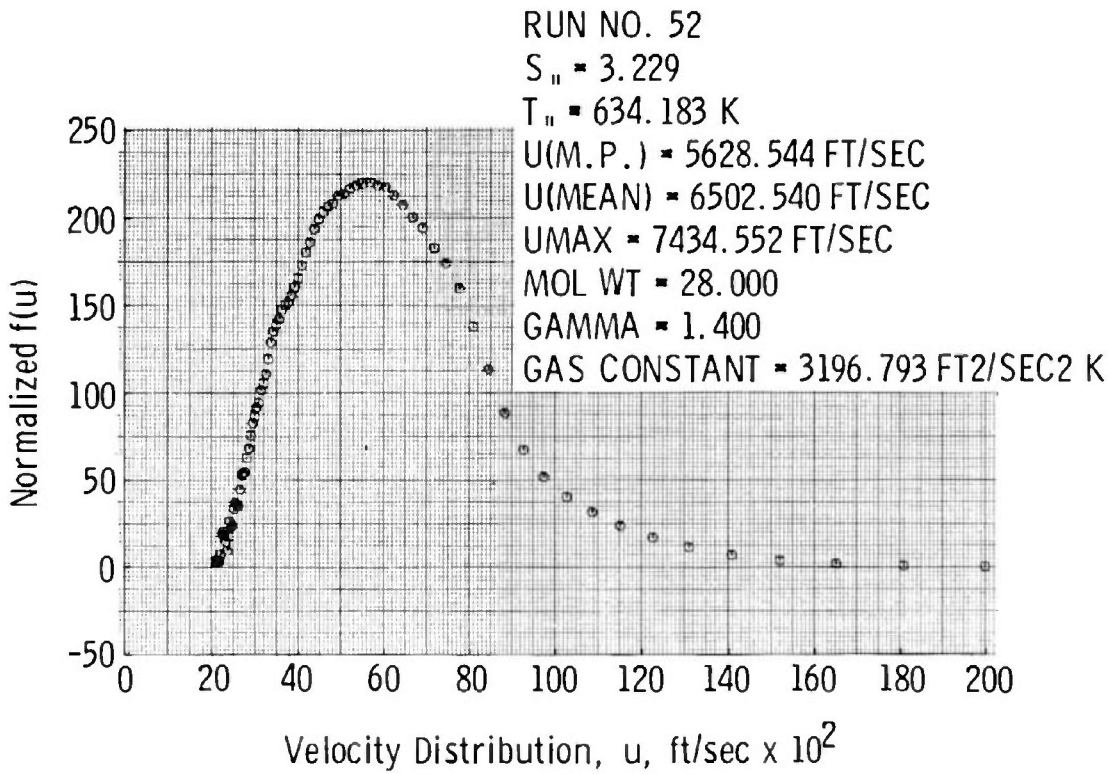

b. Velocity Distribution
Fig. 31 Concluded

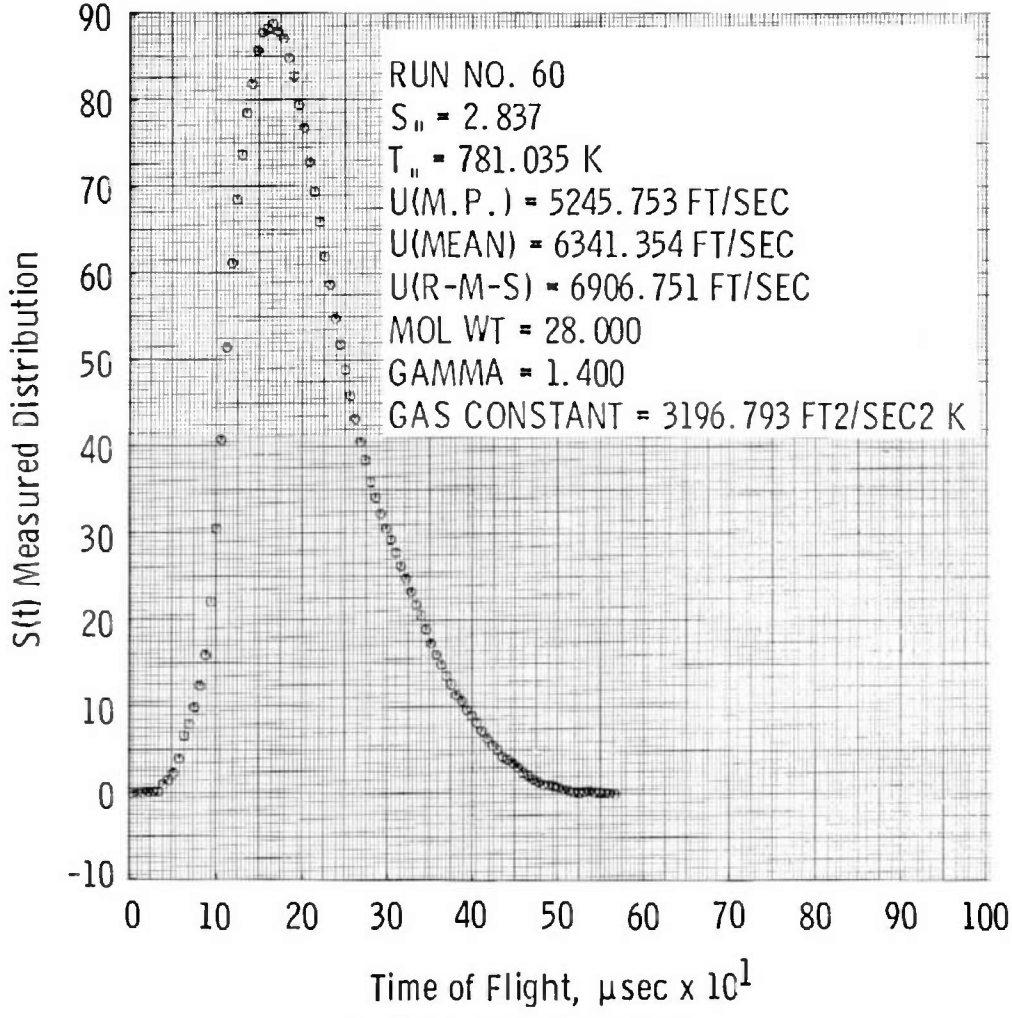

a. Time-of-Flight Distribution

Fig. 32 Nitrogen Time-of-Flight and Velocity Measurement for Hot Thruster Firing, U_{mp} = 5246 ft/sec

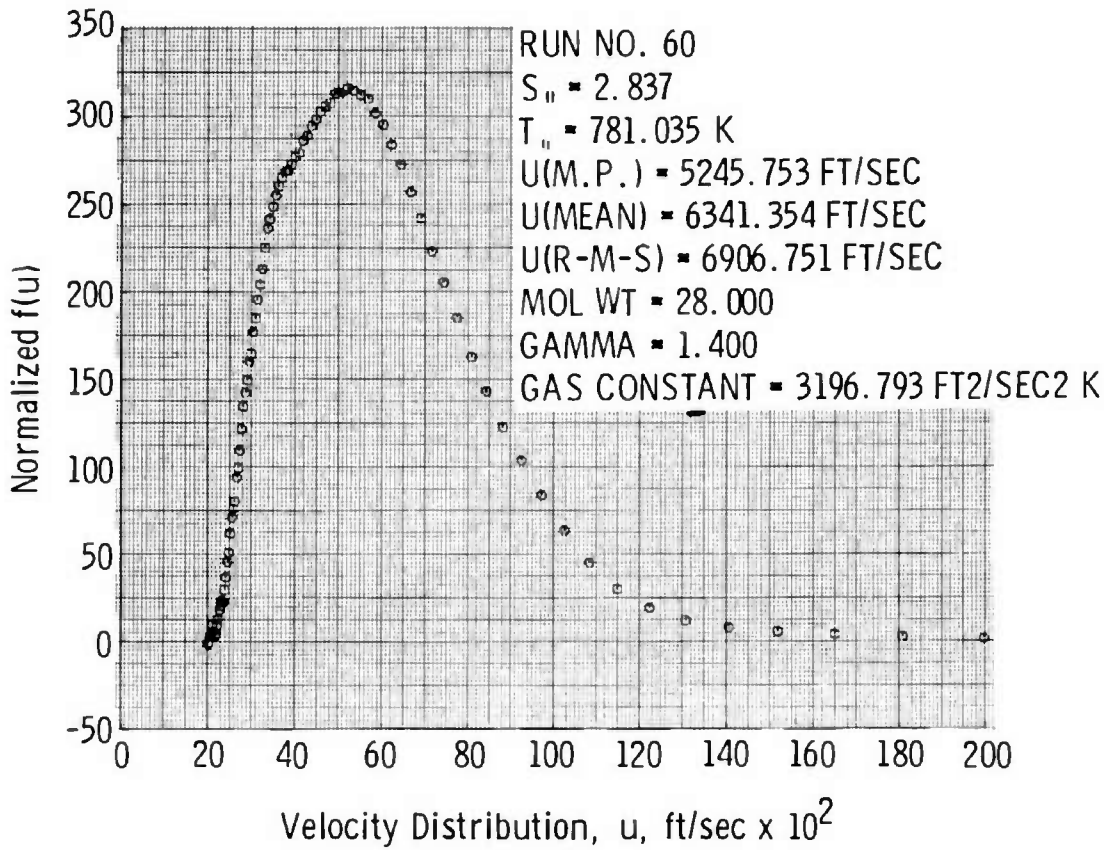

b. Velocity Distribution
Fig. 31 Concluded

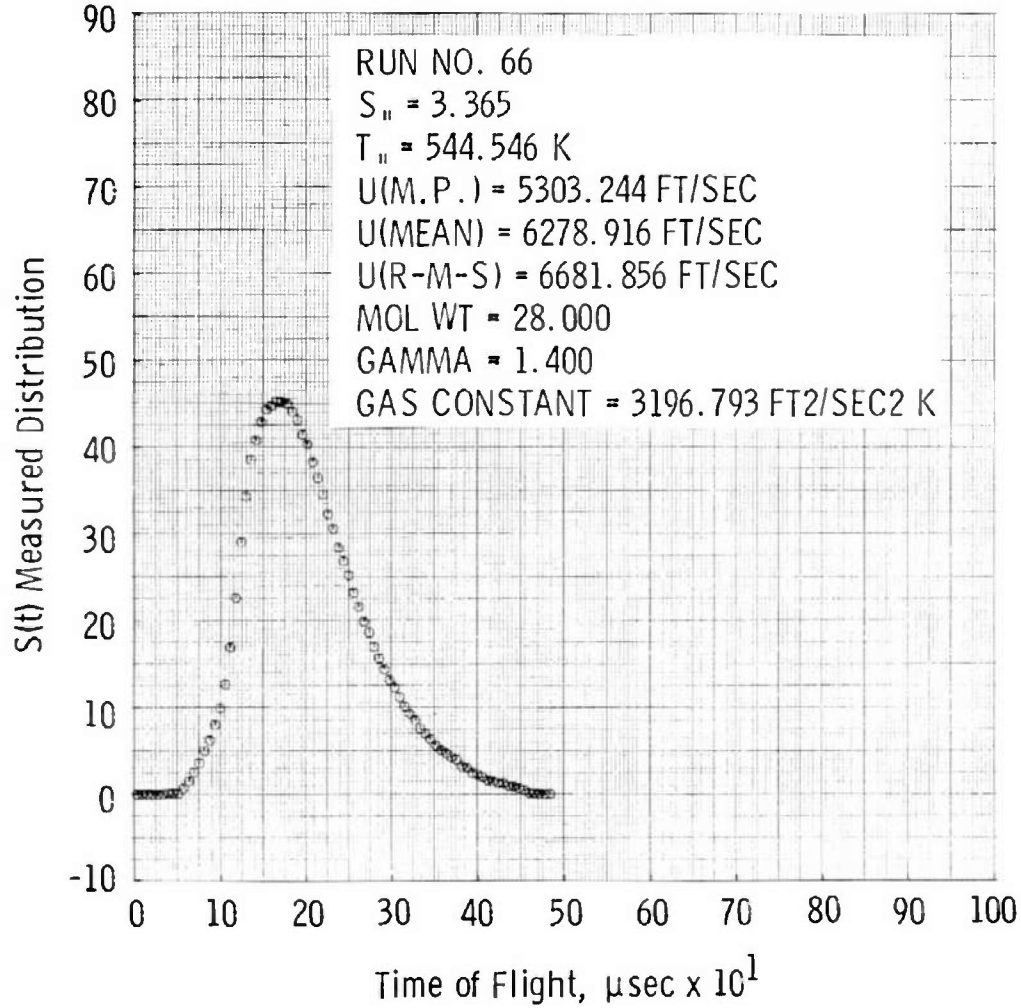

a. Time-of-Flight Distribution

Fig. 33 Nitrogen Time-of-Flight and Velocity Measurement for Hot Thruster Firing, U_{mp} = 5303 ft/sec

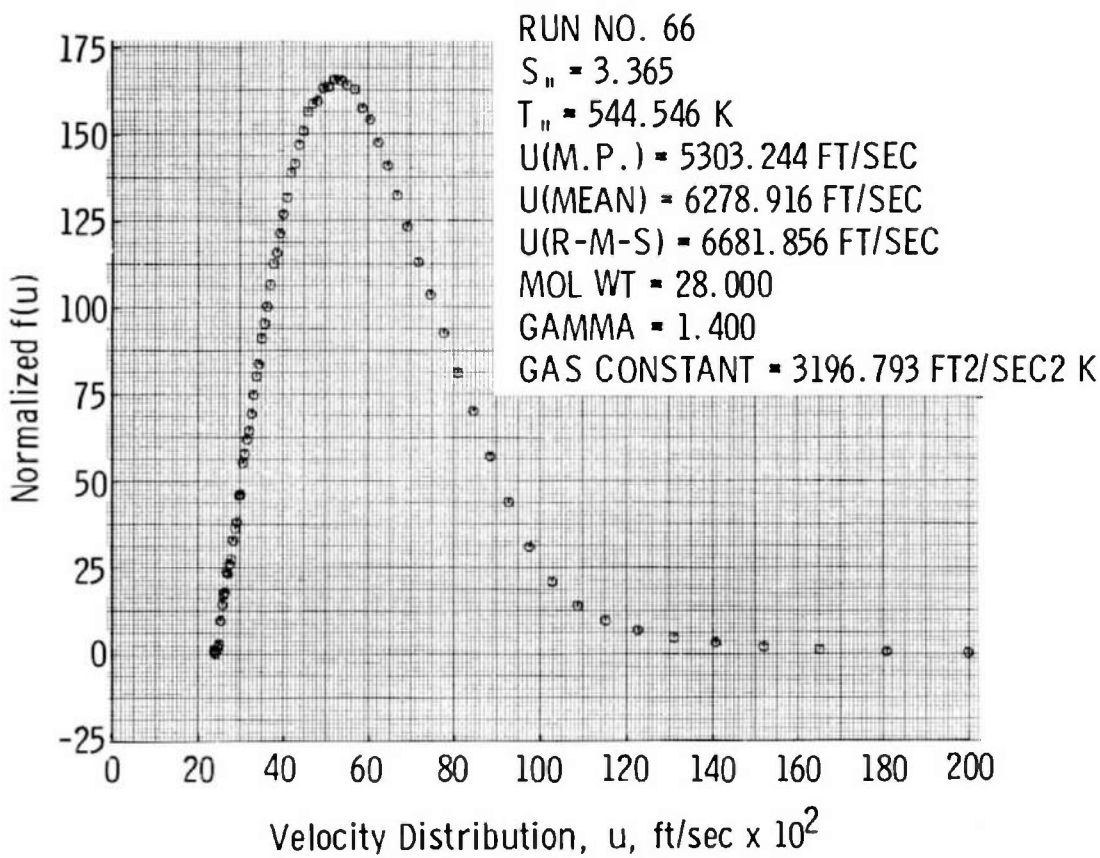

b. Velocity Distribution
Fig. 33 Concluded

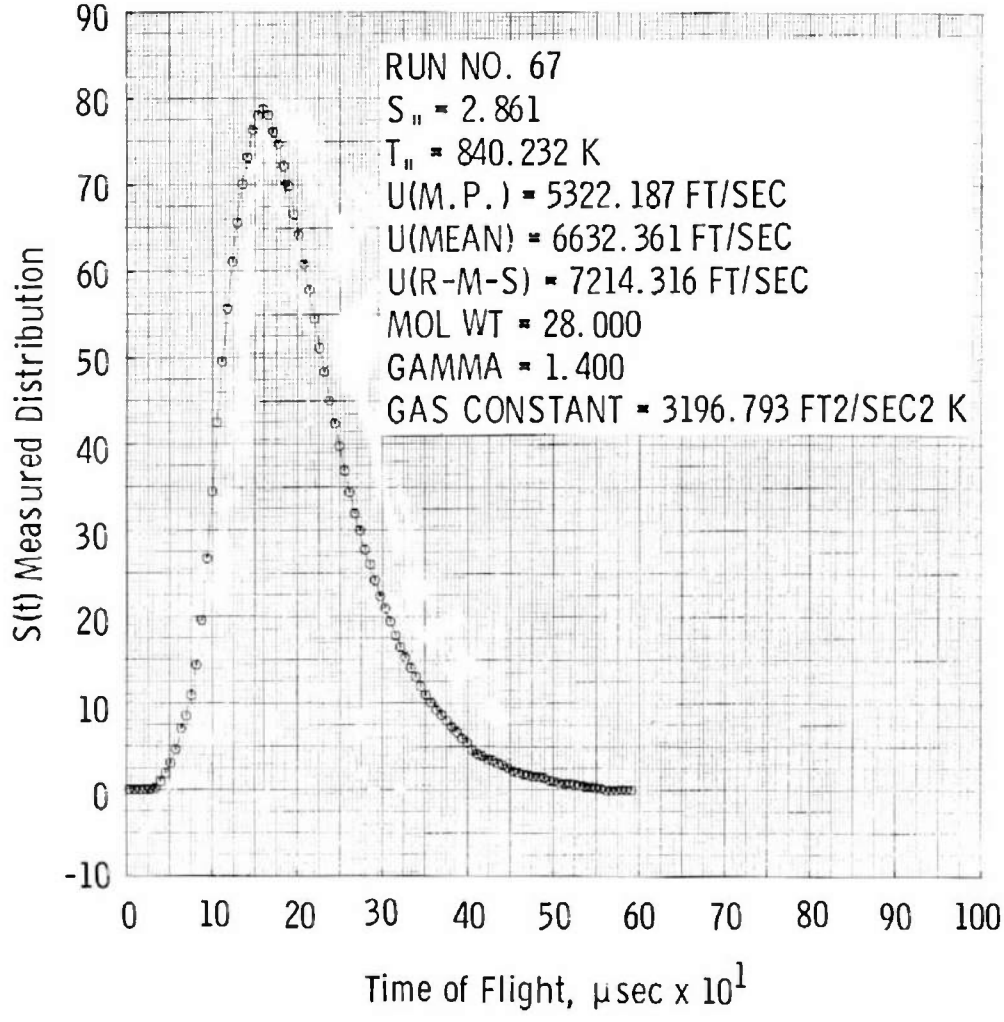

a. Time-of-Flight Distribution

Fig. 34 Nitrogen Time-of-Flight and Velocity Measurement for Hot Thruster Firing, U_{mp} = 5322 ft/sec

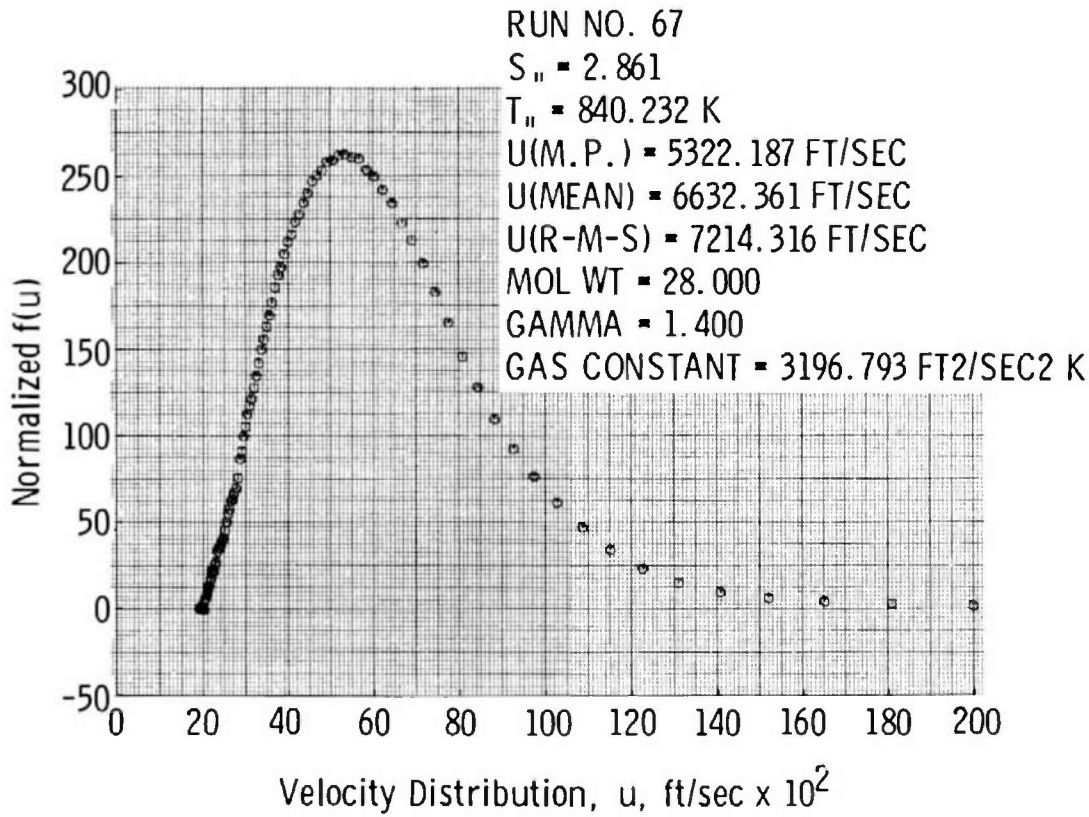

b. Velocity Distribution
Fig. 34 Concluded

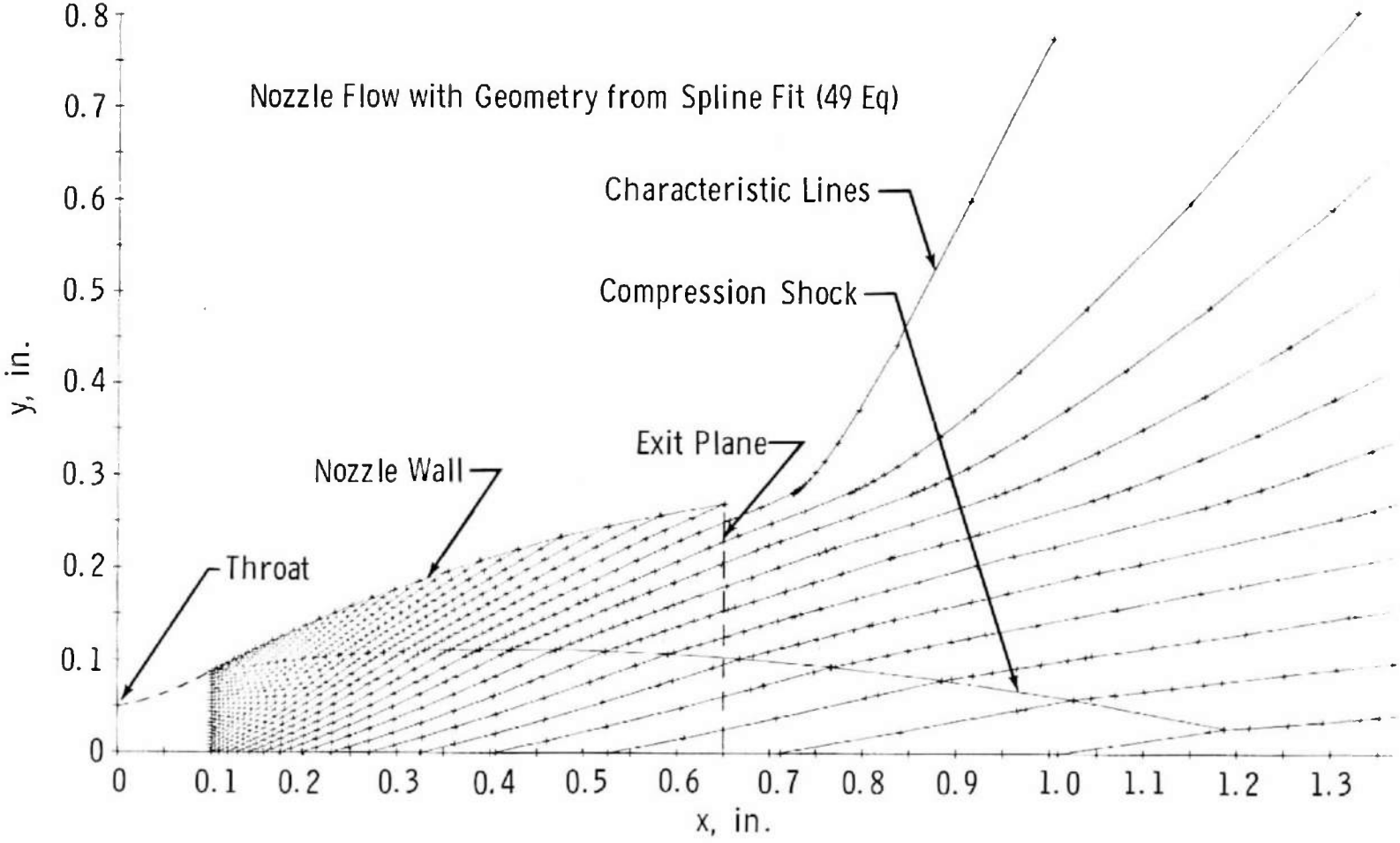

Fig. 35 Characteristic Solution Using Nozzle Geometry

APPENDIX II
DEVELOPMENT OF EQUATION FOR ANALYSIS OF TIME-OF-FLIGHT MEASUREMENTS

In order to relate the measured signal, S(t), to the free-stream velocity distribution function f(u), consider the following argument: the total number of molecules with velocities between $\vec{C}$ and $\vec{C} + d\vec{C}$ which pass the chopper wheel in Fig. 6 during the period of time Δt that the slit in the chopper wheel permits the molecules to pass is, by definition of the distribution function $f(\vec{c})$ (Ref. 16)

$$u\vec{f}(\vec{c})\, d\vec{c}\, \Delta A\, \Delta t \tag{II-1}$$

where ΔA is the area of the slit. Assuming that the probability of the distributions of the transverse components of molecular velocities, v and w, are independent of the u components, the number of molecules described by Eq. (II-1) is proportional to the number of molecules with velocities from u to u + Δu which cross ΔA during time Δt, since

$$u\vec{f}(\vec{c})d\vec{c}\Delta A\Delta t = \int_{-\infty}^{\infty}\int_{-\infty}^{\infty} u\vec{f}(\vec{c})\Delta u dv dw \Delta A \Delta t = uf(u)\Delta u \Delta A \Delta t \tag{II-2}$$

The number of molecules which cross ΔA (chopper slit) during time Δt with velocities u to u + Δu, Eq. (II-2), is also proportional to the number of molecules with velocities from u to u + Δu in the ionization region at some time t. Since the signal S(t) is also proportional to the number of molecules in the ionization region at some time t, it follows that

$$S(t) = uf(u)\, \Delta u\, \Delta A\, \Delta t \tag{II-3}$$

The range of the velocities of the molecules in the ionization region is necessarily the difference between the fastest ones, whose velocities cannot exceed $\frac{\ell + \Delta\ell}{t}$ ($\Delta\ell$ is the length of the ionization region), and the slowest ones, whose velocities must be at least $\frac{\ell}{t}$. Therefore,

$$\Delta u = \frac{\ell + \Delta\ell}{t} - \frac{\ell}{t} = \frac{\Delta\ell}{t} \tag{II-4}$$

Substituting Eq. (II-4) into Eq. (II-3) one has

$$S(t) = \frac{\ell}{t} f\left(\frac{\ell}{t}\right)\frac{\Delta\ell}{t}\, \Delta A\, \Delta t \tag{II-5}$$

of since ℓ, $\Delta\ell$, ΔA, and Δt are constant

$$t^2 S(t) = f\left(\frac{\ell}{t}\right) \tag{II-6}$$

Gas Properties

Using the assumptions that (1) the probability of the distributions of the transverse components of molecular velocity are independent of the parallel components, and (2) that $f(u) \equiv 0$ for $u < 0$, one has for the mean free-stream velocity in the x direction

$$\bar{u} = \frac{\int_0^\infty u f(u)\, du}{\int_0^\infty f(u)\, du} = \frac{\int_0^\infty \frac{\ell S(t)}{t}\, dt}{\int_0^\infty S(t)\, dt} \tag{II-7}$$

and for the average of the square of the free-stream velocity

$$\overline{u^2} = \frac{\int_0^\infty u^2 f(u)\, du}{\int_0^\infty f(u)\, du} = \frac{\int_0^\infty \frac{\ell^2 S(t)}{t^2}\, dt}{\int_0^\infty S(t)\, dt} \tag{II-8}$$

The translational kinetic temperature, T, is defined by (Ref. 16)

$$\frac{3}{2} KT = \frac{1}{2} M \overline{\left[(u-\bar{u})^2 + (v-\bar{v})^2 + (w-\bar{w})^2\right]} \tag{II-9}$$

and since $v = w = 0$

$$\frac{3}{2} KT = \frac{1}{2} M \overline{\left[(u-\bar{u})^2 + u^2 + w^2\right]} \tag{II-10}$$

which can be written

$$\frac{3}{2} KT = \frac{1}{2} M \left[\overline{(u-\bar{u})^2} + \overline{v^2} + \overline{w^2}\right] \tag{II-11}$$

Define

$$\frac{3}{2} KT_{\parallel} = \frac{1}{2} M \overline{(u-\bar{u})^2} \tag{II-12}$$

and

$$\frac{3}{2} KT_{\perp} = \frac{1}{2} M (\overline{v^2} - \overline{w^2}) \tag{II-13}$$

Note that these temperatures depend upon translational energy only, and have nothing to do with internal energy. It is predicted in Refs. 17 through 19 that $T_{\parallel} > T_{\perp}$ in highly expanded flows. In fact, in some cases, $T_{\parallel}$ may be more than an order of magnitude larger than $T_{\perp}$

(Ref. 18). Therefore, since only the u components of velocity have been measured, only the parallel temperature $T_{\parallel}$ can be calculated directly. Expanding the right-hand side of Eq. (II-12) one obtains for $T_{\parallel}$

$$RT_{\parallel} = \frac{1}{3}\left[\overline{u^2} - (\bar{u})^2\right] \tag{II-14}$$

From the definition of speed ratio one obtains

$$S = \frac{\bar{u}}{\sqrt{2RT_{\parallel}}} = \frac{\bar{u}}{\left\{\frac{2}{3}\left[\overline{u^2} - (\bar{u})^2\right]\right\}^{1/2}} = \left\{\frac{2}{3}\left[\frac{\overline{u^2}}{(\bar{u})^2} - 1\right]\right\}^{-1/2} \tag{II-15}$$

TABLE I
NOZZLE CONTOUR OF 1-LB THRUSTER

X, in.	Y, in.
0.000	0.04642
0.010	0.04642
0.020	0.04675
0.030	0.04853
0.040	0.05196
0.050	0.05759
0.060	0.06341
0.070	0.06972
0.080	0.07561
0.090	0.08142
0.100	0.08811
0.150	0.11389
0.200	0.13735
0.256	0.15862
0.300	0.17703
0.350	0.19459
0.400	0.21019
0.450	0.22587
0.500	0.23892
0.550	0.24943
0.600	0.25963
0.650	0.26866
0.700	0.27865
0.750	0.29084

TABLE II
THEORETICAL COMPOSITION OF MMH/N_2O_4 EXHAUST PLUME IN CHEMICAL EQUILIBRIUM

Component	Typical Concentration in Mole Fractions
H_2O	0.3343
N_2	0.3075
CO	0.1287
H_2	0.1576
CO_2	0.0401
OH	0.0111
H	0.0179
O_2	0.0007
NO	0.0013
O	0.0008

UNCLASSIFIED
Security Classification

DOCUMENT CONTROL DATA - R & D

(Security classification of title, body of abstract and indexing annotation must be entered when the overall report is classified)

1 ORIGINATING ACTIVITY (Corporate author)
Arnold Engineering Development Center
ARO, Inc., Operating Contractor
Arnold Air Force Station, Tennessee 37389

2a. REPORT SECURITY CLASSIFICATION
UNCLASSIFIED

2b. GROUP
N/A

3 REPORT TITLE
EVALUATION OF A MASS SPECTROMETER PROBE FOR DENSITY AND VELOCITY DISTRIBUTION MEASUREMENTS IN A ROCKET EXHAUST PLUME

4. DESCRIPTIVE NOTES (Type of report and inclusive dates)
Final Report, October 17, 1969, to June 1970

5. AUTHOR(S) (First name, middle initial, last name)
H. M. Powell, D. W. Hill, and D. L. Whitfield, ARO, Inc.

6 REPORT DATE	7a. TOTAL NO OF PAGES	7b. NO. OF REFS
September 1971	82	19

8a. CONTRACT OR GRANT NO	9a. ORIGINATOR'S REPORT NUMBER(S)
F40600-71-C-0002	
b. PROJECT NO.	AEDC-TR-71-135
c. Program Element 64719F	9b. OTHER REPORT NO(S) (Any other numbers that may be assigned this report)
d.	ARO-VKF-TR-71-50

10 DISTRIBUTION STATEMENT
Approved for public release; distribution unlimited.

11 SUPPLEMENTARY NOTES	12 SPONSORING MILITARY ACTIVITY
Available in DDC.	Arnold Engineering Development Center (AFSC), Arnold Air Force Station, Tennessee 37389

13 ABSTRACT

The evaluation of a mass spectrometer probe in a highly expanded exhaust plume of a small rocket is described in this report. This probe, which utilizes a quadrupole mass spectrometer, is used for species identification and concentration measurements and for velocity distribution measurements. The probe maintains a compatible pressure environment for the spectrometer during rocket firings and generates a molecular beam which is representative of the plume gas dynamic state at a given sampling point. The modulated beam technique for both density and velocity distribution measurements is described. The important criteria for the design of the more important features are discussed. Sample data from calibration sources and the thruster are presented along with analysis of the data as it relates to parameter spatial dependence and kinetic temperatures calculated from the velocity distributions.

DD FORM 1 NOV 65 1473

UNCLASSIFIED
Security Classification

14. KEY WORDS	LINK A		LINK B		LINK C	
	ROLE	WT	ROLE	WT	ROLE	WT
mass spectrometer						
performance evaluation						
rocket engines						
plumes						
space simulation						
density						
velocity						